

A robust control strategy for a self-excited induction generator wind turbine system

Godpromesse Kenne¹ · Clotaire Thierry Sanjong^{1,2} · Armel Simo Fotso^{1,2} · Eustace Mbaka Nfah^{1,3}

Received: 6 September 2016 / Revised: 6 September 2016 / Accepted: 3 November 2016 / Published online: 29 November 2016
© Springer-Verlag Berlin Heidelberg 2016

Abstract In this paper, a new control strategy of a variable speed based SEIG wind energy conversion is presented. Nonlinear control strategy is proposed to extract maximum available energy from the wind turbine and regulate the rotor flux magnitude of SEIG and the DC-link voltage in the generator side as well as the load voltage magnitude in the inverter load side under wind speed, load and rotor/stator resistances variations. The proposed nonlinear adaptive controller is robust given its insensitivity to SEIG variation of the rotor and stator resistances. The global convergence and stability analysis taking into account the interconnections between the stator electrical angular position, the rotor flux and rotor resistance estimators and the nonlinear controller have been proved by using the separation principle. Another contribution of this paper is the robustness of the proposed method with respect to the variation of the driven speed and relatively low wind speed operation. Thus, the proposed

stand-alone variable speed based SEIG wind energy conversion system can be used in remote and isolated areas where the mean value of the wind speed profile is relatively low.

Keywords MPPT · PWM converter · Voltage regulation · Nonlinear control · Time-varying parameter estimation

1 Introduction

1.1 Antecedents and motivations

The self-excited induction generator (SEIG) has emerged from among the well known generators as a suitable candidate to be driven by wind turbine. The main advantages of the SEIG are small size and weight, low cost and simplicity of construction, absence of separate source for excitation and reduced maintenance cost but its main drawback is its inherently poor voltage regulation. The fact that the induction machine (IM) is a multivariable, nonlinear and highly coupled process with time-varying parameters, has motivated a lot of work in the control community during the last decade [1–17]. The most popular method is the field-oriented control (F.O.C.) which provides a means to obtain high-performance control of IM. But F.O.C. methodology requires knowledge of the rotor flux which is not usually measured [14]. Traditionally, observers are used to estimate the rotor flux. However, the flux observers used in the currently IM control rely on a good knowledge of the rotor resistance.

It is well known in literature (e.g. see [1–17]) that the rotor resistance and the stator resistance may vary up to 100% and 50% of their nominal values, respectively, during operation of the IM due to rotor heating. Standard methods for the estimation of IM parameters include the blocked rotor test, the no-load test and the standstill frequency response test. But,

✉ Godpromesse Kenne
gokenne@yahoo.com;
godpromesse.kenne@univ-dschang.org

Clotaire Thierry Sanjong
sanjongthierry@yahoo.fr

Armel Simo Fotso
fotsimmo@yahoo.fr

Eustace Mbaka Nfah
emnfah@yahoo.com

¹ Laboratoire d'Automatique et d'Informatique Appliquée (LAIA), Département de Génie Electrique, Université de Dschang, B.P. 134, Bandjoun, Cameroon

² Laboratoire d'Electronique et de Traitement de Signal (LETS), Département de Physique, Université de Dschang, B.P. 69, Dschang, Cameroon

³ Higher Technical Teacher Training College (HTTC) Bambili - Bamenda, Department of Power and Electrical Engineering, University of Bamenda, Bamenda, Cameroon

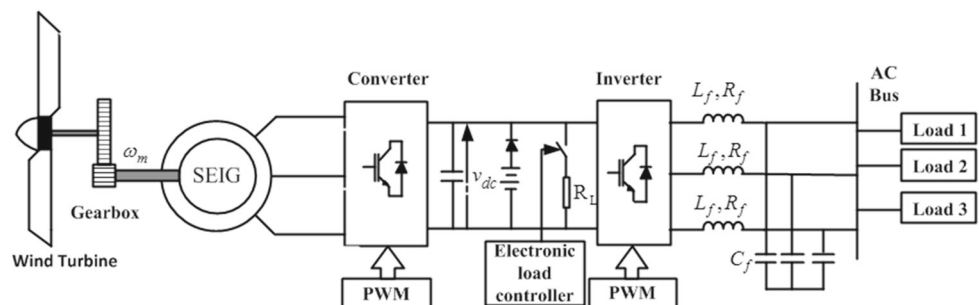
these methods cannot be used online during normal operation of the machine. The most natural solution is to online identify the time-varying parameters. The problem of the online identification of the induction machine parameters has been addressed by several papers in the literature [1–17].

But in the self-excited generator mode operation of the IM, different approaches for voltage regulation have been developed [18–20] without taking into account the fact that the rotor resistance required for the rotor flux estimation is time-varying. In [19] the technique and limitation of varying the flux in the induction generator to regulate the generated voltage under variation of the rotor speed are discussed. In [18], standard sliding mode control associated to the flux oriented control technique is applied to the dc-bus voltage regulation of SEIG. The control strategy proposed in [18] is difficult to implement online because this method used the rotor flux and the rotor resistance which varies with the operating conditions. In [20], fuzzy logic based voltage controller has been proposed for voltage source pulse width modulation (PWM) converter connected to SEIG to regulate the dc-bus voltage. In the above contributions, the investigation of the variation of the electrical parameters (e.g. stator and rotor resistance) has not been discussed.

1.2 Main contributions

In this paper, a new control strategy of a stand-alone variable speed based SEIG wind energy conversion is presented. The main objective of the proposed adaptive nonlinear control strategy is to extract maximum available energy from the wind turbine and regulate the rotor flux magnitude of SEIG and the DC-link voltage in the generator side as well as the load voltage magnitude in the inverter load side under wind speed, load and rotor/stator resistances variations. To this end, adaptive nonlinear controllers are designed. In order to avoid the chattering effect, we used an approximation of the sign function of the well known sliding mode control technique which has proved to be particularly appropriate for nonlinear systems control, presenting robust features with respect to system parameter uncertainties and external disturbances [21].

Fig. 1 Global structure of the control system



The proposed nonlinear adaptive controller is robust given its insensitivity to SEIG variation of the rotor resistance and stator resistance. The global convergence and stability analysis taking into account the interconnections between the stator electrical angular position, the rotor flux and rotor resistance estimators and the nonlinear controller have been proved by using the separation principle. The resulting nonlinear controllers can be easily implemented in practice since finite time estimators for the rotor resistance, rotor flux and stator electrical angular position required for the adaptation of the controller are provided.

Another contribution of this paper is the robustness of the proposed method with respect to the variation of the driven speed and relatively low wind speed operation. Consequently, the proposed stand-alone variable speed based SEIG wind energy conversion system can be used in remote and isolated areas where the mean value of the wind speed profile is relatively low.

1.3 Structure of the paper

The paper is organized as follows. In Sect. 2, global structure and control objective are presented. In Sect. 3, generator side control strategy is described while in Sect. 4, load side inverter control strategy design is introduced. In Sect. 5, simulation results using the proposed nonlinear controller and conventional P.I. controllers are reported and some concluding remarks are given in Sect. 6.

2 Global structure and control objective

The control structure of a SEIG based variable speed wind turbine is shown in Fig. 1. This structure consists of the SEIG connected to a variable speed wind turbine through a step-up gear box, a PWM controlled converter and a vector controlled PWM voltage source inverter which is used to supply the loads through LC filter. It can be noticed that the output of a variable speed SEIG can not be used without transformation as it varies in amplitude and frequency due to fluctuating wind. Thus, a constant dc-voltage is required for direct use, storage or conversion to AC via an inverter.

Initially, the dc-bus voltage is assumed to be zero and the battery on the dc-bus side of the inverter provides the initial excitation through the diode. When the rotor flux reaches the desired level, the dc-bus voltage increases and becomes greater than the battery voltage; Then the diode cuts off the battery from the dc-bus and the generator supplies itself the necessary energy to control the voltage across the compensator dc-capacitor and the reactive power required by the SEIG is provided by the three-phase control converter.

The goal of this work is to use a simple maximum power point tracking strategy to extract the optimal torque of the variable speed turbine and design the dc-voltage and rotor flux controllers as well as the load side frequency and voltage regulators assuming that the measured outputs are the rotor speed, stator currents, load-side currents and voltages despite large variation of the stator/rotor resistances.

3 Generator side control strategy

The control task in this section is to extract the maximum power from the wind turbine and regulate the rotor flux and the dc-bus voltage.

3.1 Modeling of the wind turbine

The mechanical power extracted from wind turbine can be expressed as:

$$P_t = \frac{1}{2} \pi \rho R^2 C_p(\lambda) v^3 \tag{1}$$

where ρ is the air density, R is the radius of the turbine, v is the wind speed, $C_p(\lambda)$ is the power coefficient and λ is the tip-speed ratio (TSR). This TSR is given by the relation

$$\lambda = \frac{R\omega_{mt}}{v} = \frac{R\omega_m}{n_g v} \tag{2}$$

where ω_{mt} is the turbine rotor speed, ω_m is the generator rotor speed and n_g is the gearbox ratio. The general characterization of C_p depends on λ and the blade pitch angle β . In the literature, many authors have proposed different methods to characterize the expression of $C_p(\lambda)$ [22,23]. All the analysis in this work is done considering the angle of the blade pitch β settled to zero, i.e. $\beta \equiv 0$. The following characterization taken from [23] is used.

$$C_p(\lambda) = \left(\frac{C_2}{\lambda} - C_3 \right) e^{-\frac{C_1}{\lambda}} + C_4 \lambda. \tag{3}$$

Maximum power can be extracted from the wind turbine when it operates at maximum C_p (i.e at C_p^*) [23]. This is achieved if the rotor speed is kept at an optimal value of the

TSR λ^* . The optimal rotor speed can be obtained by solving Eq. (2) for ω_{mt} :

$$\omega_{mt}^* = \frac{\lambda^* v}{R}. \tag{4}$$

Therefore, for a given wind speed, the main control objective is to regulate the rotor speed to its optimal value.

The rotor dynamic of wind turbine system is given by:

$$J_t \frac{d\omega_m}{dt} = \frac{T_t}{n_g} - T_e - f\omega_m, \tag{5}$$

where J_t is the turbine total inertia, T_t is the aerodynamic torque, and f is the turbine total external damping. The wind turbine characteristics used in this work is given in ‘‘Appendix 4’’.

3.2 Modeling of the induction generator

Assuming that the rotor flux is oriented such the quadrature component $\phi_{rq} = 0$, the dynamic model of the induction generator associated to PWM converter in the synchronously rotating reference frame d and q axis is given by [18,24]:

$$\dot{i}_{sd} = -\gamma_1 i_{sd} + \omega_s i_{sq} + \gamma_2 \phi_r + v v_{sd} \tag{6}$$

$$\dot{i}_{sq} = -\omega_s i_{sd} - \gamma_1 i_{sq} - \gamma_3 \omega \phi_r + v v_{sq} \tag{7}$$

$$\dot{\phi}_r = \frac{L_m}{\tau_r} i_{sd} - \frac{1}{\tau_r} \phi_r \tag{8}$$

$$\omega_s = \omega + \omega_r, \quad \omega_r = \frac{L_m}{\tau_r} \frac{i_{sq}}{\phi_r}, \quad \theta_s = \int \omega_s dt \tag{9}$$

$$v_{sd} = \frac{1}{2} S_d v_{dc}, \quad v_{sq} = \frac{1}{2} S_q v_{dc}, \quad T_e = n_p \frac{L_m}{L_r} \phi_r i_{sq} \tag{10}$$

$$\dot{v}_{dc} = -\frac{1}{2C} (S_d i_{sd} + S_q i_{sq}) - \frac{S v_{dc}}{R_L C} - \frac{i_i}{C}$$

with $\sigma = 1 - \frac{L_m^2}{L_s L_r}$, $\tau_s = \frac{L_s}{R_s}$, $\tau_r = \frac{L_r}{R_r}$, $v = \frac{1}{\sigma L_s}$

$$\gamma_1 = \frac{1}{\sigma \tau_s} + \frac{1 - \sigma}{\sigma \tau_r}, \quad \gamma_2 = \frac{1 - \sigma}{L_m \sigma \tau_r}, \quad \text{and} \quad \gamma_3 = \frac{1 - \sigma}{L_m \sigma}. \tag{11}$$

The first expression of (9) represents the relation between the stator voltages/ currents electrical angular frequency ω_s and the rotor currents electrical angular frequency ω_r while the last expression is the stator electrical angular position θ_s . The notation for the nonlinear dynamics of induction generator is given in ‘‘Appendix 7’’. The measured variable is ω , while (i_{sd}, i_{sq}) , ϕ_r and R_r are not measurable. The control inputs are the stator voltages (v_{sd}, v_{sq}) and the outputs to be controlled are the rotor flux ϕ_r , the generator rotor speed ω_m and the dc-voltage v_{dc} in the dc-side.

Note that the rotor and stator winding resistances are typically uncertain because R_r and R_s may vary up to 100% and

50% of their nominal values, respectively due to stator and rotor heating.

The following assumptions will be considered until further notice.

- (i) The stator current and voltage are bounded signals.
- (ii) The rotor resistance $R_r \in \Omega_{R_r}$, where Ω_{R_r} is a compact set of \mathbb{R} .
- (iii) It is also assumed that the rate of variation of the stator/rotor inductances (L_m, L_s, L_r) and rotor resistance are negligible compared to the dynamic of the stator currents and the rotor flux.

The control objectives of the generator side can be summarized as follows:

- Achievement of the maximum energy extraction by regulating the the rotor speed to its optimal value,
- Regulation of the dc-bus voltage and rotor flux,

for any unknown but bounded R_r , despite uncertainties on the stator resistance.

Remark 1 The values of (i_{sd}, i_{sq}) can be computed using the measurements of the stator currents (i_{sa}, i_{sb}, i_{sc}) , the estimation of the stator electrical angular position θ_s and the (a, b, c) coordinate frame $\rightarrow (d, q)$ coordinate frame transformation. The expression used for the estimation of θ_s is given in Sect. 3.4.2 and the (a, b, c) coordinate frame $\rightarrow (d, q)$ coordinate frame transformation is given in ‘‘Appendix 8’’.

3.3 Non-adaptive control strategy

Since Eqs. (5) and (8) do not contain the stator voltage explicitly as an input, in the following analysis, some transformations will be done to make the stator voltage components v_{sd} and v_{sq} appear explicitly as inputs in both equations.

Under *assumptions (i)–(iii)*, we first compute the second time-derivative of ϕ_r and then use (6) and (8) to derive the dynamic equation for the rotor flux containing the stator voltage component v_{sd} as a control input. We then obtain

$$\begin{aligned} \frac{d^2\phi_r}{dt^2} &= f_{\phi_r} + a_4 v_{sd} \\ \text{with } f_{\phi_r} &= a_1 i_{sd} + a_2 i_{sq} + a_3 \phi_r, \\ a_1 &= -\left(\frac{L_m \gamma_1}{\tau_r} + \frac{L_m}{\tau_r^2}\right), a_2 = \frac{L_m \omega_s}{\tau_r}, \\ &\times a_3 = \frac{L_m \gamma_2}{\tau_r^2} + \frac{1}{\tau_r}, a_4 = \frac{\nu L_m}{\tau_r}. \end{aligned} \tag{12}$$

To derive the dynamic equation for the rotor speed containing the stator voltage component v_{sq} as a control input, let us rewrite (5) as follows.

$$\frac{d\omega_m}{dt} = \frac{T_t}{J_t n_g} - \frac{T_e}{J_t} - \frac{f}{J_t} \omega_m, \tag{13}$$

Since the aerodynamic torque T_t is not measurable and the control strategy is to derive the controller that ensures optimal torque tracking in finite time, we exploit the work of [25] and replace T_t in (13) by the following expression:

$$T_{top} = k_{op}(\omega_m)^2 \quad \text{with} \quad k_{op} = \frac{\rho \pi R^5 C_p^*}{2\lambda^3 n_g^2}. \tag{14}$$

The dynamic equation for the rotor speed containing the stator voltage component as a control input is derived by computing the second time-derivative of ω_m and using (13), (7) and (10). This leads to

$$\begin{aligned} \frac{d^2\omega_m}{dt^2} &= f_{\omega_m} + b_9 v_{sq}, \\ \text{with } f_{\omega_m} &= b_1 \omega_m^3 + b_2 \omega_m^2 + b_3 \omega_m + b_4 \omega_m \phi_r i_{sq} \\ &\quad + b_5 \phi_r i_{sq} + b_6 i_{sd} i_{sq} + b_7 \omega_s \phi_r i_{sd} + b_8 \omega_m \phi_r^2, \\ b_1 &= \frac{2k_{op}^2}{J_t^2 n_g^2}, \quad b_2 = \frac{3fk_{op}}{J_t^2 n_g}, \quad b_3 = \frac{f^2}{J_t^2}, \\ b_4 &= \frac{-2n_p L_m k_{op}}{J_t^2 n_g L_r}, \quad b_5 = \frac{n_p L_m}{J_t L_r} \left(\frac{f}{J_t} + \frac{1}{\tau_r} + \gamma_1\right) \\ b_6 &= \frac{-n_p L_m^2}{J_t L_r \tau_r}, \quad b_7 = \frac{n_p L_m}{J_t L_r}, \quad b_8 = \frac{n_p^2 \gamma_3 L_m}{J_t L_r}, \\ b_9 &= \frac{-n_p L_m \nu \phi_r}{J_t L_r}. \end{aligned} \tag{15}$$

Remark 2 Since v_{sd} and v_{sq} given by (12) and (15) are responsible for the flux magnitude control and rotor speed control, respectively, the control goals can now be viewed as a decoupling problem.

Assuming that the rate of variation of the rotor flux and rotor speed references signals are negligible compared to other existing dynamics, the rotor flux and rotor speed tracking error dynamics are given by

$$\ddot{e}_{\phi_r} = -f_{\phi_r} - a_4 v_{sd} \tag{16}$$

$$\ddot{e}_{\omega_m} = -f_{\omega_m} - b_9 v_{sq}. \tag{17}$$

Under the assumption that the rotor flux and rotor resistance are available, let us choose the switching surfaces [26] ($c_{\phi_r} >$

0 and $c_{\omega_m} > 0$ are tuning parameters)

$$s_{\phi_r} = \frac{de_{\phi_r}}{dt} + c_{\phi_r} e_{\phi_r} \tag{18}$$

$$s_{\omega_m} = \frac{de_{\omega_m}}{dt} + c_{\omega_m} e_{\omega_m}, \text{ with } e_{\omega_m} = \omega_m^* - \omega_m \tag{19}$$

and the Lyapunov candidate function

$$W = \frac{1}{2}(a_4 s_{\phi_r}^2 + b_9 s_{\omega_m}^2) \tag{20}$$

whose time-derivative is:

$$\dot{W} = a_4 s_{\phi_r} \dot{s}_{\phi_r} + b_9 s_{\omega_m} \dot{s}_{\omega_m}. \tag{21}$$

By choosing ($k_{v_{sd}}$ and $k_{v_{sq}}$ are positive design parameters)

$$v_{sd} = v_{sdeq} - k_{v_{sd}} \text{sign}(s_{\phi_r}) \tag{22}$$

$$v_{sq} = v_{sqeq} - k_{v_{sq}} \text{sign}(s_{\omega_m}) \tag{23}$$

where

$$v_{sdeq} = \frac{1}{a_4} \left[f_{\phi_r} + c_{\phi_r} \left(\frac{L_m}{\tau_r} i_{sd} - \frac{1}{\tau_r} \phi_r \right) \right], \tag{24}$$

$$v_{sqeq} = -\frac{1}{b_9} \left[f_{\omega_m} + c_{\omega_m} (k_{opt} \omega_m^2 - \frac{n_p L_m}{L_r} \phi_r i_{sq} - f \omega_m) \right] \tag{25}$$

are equivalent control terms [27] and are the unique solutions of $\dot{s}_{\phi_r} = 0$ and $\dot{s}_{\omega_m} = 0$ respectively, the time-derivative of W becomes

$$\dot{W} = -k_{v_{sd}} a_4 |s_{\phi_r}| - k_{v_{sq}} b_9 |s_{\omega_m}|. \tag{26}$$

Therefore, $|s_{\phi_r}| \rightarrow 0$ and $|s_{\omega_m}| \rightarrow 0$ which implies that $|e_{\phi_r}|$ and $|e_{\omega_m}|$ converge to zero. Consequently, maximum energy extraction from wind turbine is achieved by virtue of relation (4).

To prove the finite time convergence of s_{ϕ_r} to zero and s_{ω_m} to zero, we rewrite (20) as follows

$$W = W_1 + W_2$$

$$\text{with } W_1 = \frac{1}{2} a_4 s_{\phi_r}^2 \text{ and } W_2 = \frac{1}{2} b_9 s_{\omega_m}^2. \tag{27}$$

By taking into account (22)–(23) and (24)–(25), we obtain

$$s_{\phi_r} \dot{s}_{\phi_r} = -k_{v_{sd}} |s_{\phi_r}| \text{ and } s_{\omega_m} \dot{s}_{\omega_m} = -k_{v_{sq}} |s_{\omega_m}|. \tag{28}$$

The above equations can be rewritten as

$$\dot{W}_1 = -\sqrt{2} k_{v_{sd}} \sqrt{W_1(s_{\phi_r})} \text{ and } \dot{W}_2 = -\sqrt{2} k_{v_{sq}} \sqrt{W_2(s_{\omega_m})}. \tag{29}$$

Thus, there exists finite times t_{ϕ_r} and $t_{v_{sq}}$ such that inequalities (30)–(31) hold

$$t_{\phi_r} < \frac{|s_{\phi_r}(0)|}{k_{v_{sd}}} \tag{30}$$

$$t_{v_{sq}} < \frac{|s_{\omega_m}(0)|}{k_{v_{sq}}}. \tag{31}$$

The reference rotor flux linkage required at any speed is calculated using the relationship between rotor speed and rotor flux linkage as follows [19].

$$\phi_r^* = \frac{\omega_{m_{min}}}{\omega_m} \phi_{r_{max}} \tag{32}$$

Note that when the rotor speed decreases to a value lower than $\omega_{m_{min}}$, theoretically the flux linkage should increase to a value higher than $\phi_{r_{max}}$. However, in an induction machine, once the saturation level is reached, the controller forces more direct axis current i_{sd} to produce more flux. The magnitude of the exciting current can exceed the rated current of the machine without approaching the required reference flux. As a result the magnitude of the generated voltage drops.

Remark 3 To avoid the effect of the measurement noise, the time-derivatives of e_{ϕ_r} in (18) and e_{ω_m} in (19) can be computed using (8) and (5).

Note that the above nonlinear control is not implementable in practice since the slide manifold s_{ϕ_r} , the equivalent control terms (24) and (25) are not available due to the fact that the rotor flux and rotor resistance are not online measurable. Furthermore, the stator electrical angular position θ_s depends upon the rotor flux and the rotor resistance which is assumed to be unknown time-varying parameter. Consequently, on-line adaptation laws for R_r , θ_s and observer for ϕ_r are required to achieve the practical implementation of the above nonlinear controller.

3.4 Adaptive design

In this section, online estimators for the rotor resistance, rotor flux and stator electrical angular position required to achieve the implementation of the above nonlinear controller (22)–(23) are derived.

3.4.1 Rotor resistance estimation algorithm

In our approach, we adopt the dynamics of a balanced induction generator, expressed in a fixed reference frame α - β

attached to the stator [3, 28]:

$$\dot{i}_{s\alpha} = \frac{1}{\gamma_4} (-L_r R_s i_{s\alpha} + L_m^2 \omega i_{s\beta} + L_m R_r i_{r\alpha} + L_r L_m \omega i_{r\beta} + L_r v_{s\alpha}) \tag{33}$$

$$\dot{i}_{s\beta} = \frac{1}{\gamma_4} (-L_m^2 \omega i_{s\alpha} - L_r R_s i_{s\beta} - L_r L_m \omega i_{r\alpha} + L_m R_r i_{r\beta} + L_r v_{s\beta}) \tag{34}$$

$$\dot{i}_{r\alpha} = \frac{1}{\gamma_4} (L_m R_s i_{s\alpha} - L_m L_s \omega i_{s\beta} - L_s R_r i_{r\alpha} - L_s L_r \omega i_{r\beta} - L_m v_{s\alpha}) \tag{35}$$

$$\dot{i}_{r\beta} = \frac{1}{\gamma_4} (L_m L_s \omega i_{s\alpha} + L_m R_s i_{s\beta} + L_s L_r \omega i_{r\alpha} - L_s R_r i_{r\beta} - L_m v_{s\beta}) \tag{36}$$

where $\gamma_4 = L_s L_r - L_m^2$.

We can now consider the following observer ($K > 0$ is a constant designed parameter):

$$\dot{\hat{i}}_{s\alpha} = \frac{1}{\gamma_4} (-L_r R_s i_{s\alpha} + L_m^2 \omega i_{s\beta} + L_m \hat{R}_r \hat{i}_{r\alpha} + L_m L_r \omega \hat{i}_{r\beta} + L_r v_{s\alpha} + K \text{sign}(i_{s\alpha} - \hat{i}_{s\alpha})) \tag{37}$$

$$\dot{\hat{i}}_{s\beta} = \frac{1}{\gamma_4} (-L_m^2 \omega i_{s\alpha} - L_r R_s i_{s\beta} - L_m L_r \omega \hat{i}_{r\alpha} + L_m \hat{R}_r \hat{i}_{r\beta} + L_r v_{s\beta} + K \text{sign}(i_{s\beta} - \hat{i}_{s\beta})) \tag{38}$$

$$\dot{\hat{i}}_{r\alpha} = \frac{1}{\gamma_4} (L_m R_s i_{s\alpha} - L_s L_m \omega i_{s\beta} - L_s \hat{R}_r \hat{i}_{r\alpha} - L_s L_r \omega \hat{i}_{r\beta} + u_\alpha - L_m v_{s\alpha}) \tag{39}$$

$$\dot{\hat{i}}_{r\beta} = \frac{1}{\gamma_4} (L_s L_m \omega i_{s\alpha} + L_m R_s i_{s\beta} + L_s L_r \omega \hat{i}_{r\alpha} - L_s \hat{R}_r \hat{i}_{r\beta} + u_\beta - L_m v_{s\beta}) \tag{40}$$

where u_α and u_β are additional signals yet to be designed and sign is the well known sign function. The estimated quantities are shown as \hat{x} while the error quantities are given as follows $\tilde{x} = x - \hat{x}$ (e.g., $\tilde{i}_{s\alpha} = i_{s\alpha} - \hat{i}_{s\alpha}$, $\tilde{i}_{s\beta} = i_{s\beta} - \hat{i}_{s\beta}$, $\tilde{i}_{r\alpha} = i_{r\alpha} - \hat{i}_{r\alpha}$, $\tilde{i}_{r\beta} = i_{r\beta} - \hat{i}_{r\beta}$, $\tilde{R}_r = R_r - \hat{R}_r$).

The dynamics of the observer error can be computed using (33)–(36) and (37)–(40) as

$$\dot{\tilde{i}}_{s\alpha} = \frac{1}{\gamma_4} (L_m R_r \tilde{i}_{r\alpha} + L_m \tilde{R}_r \hat{i}_{r\alpha} + L_m L_r \omega \tilde{i}_{r\beta}) - K \text{sign}(\tilde{i}_{s\alpha}) \tag{41}$$

$$\dot{\tilde{i}}_{s\beta} = \frac{1}{\gamma_4} (-L_m L_r \omega \tilde{i}_{r\alpha} + L_m R_r \tilde{i}_{r\beta} + L_m \tilde{R}_r \hat{i}_{r\beta}) - K \text{sign}(\tilde{i}_{s\beta}) \tag{42}$$

$$\dot{\tilde{i}}_{r\alpha} = \frac{1}{\gamma_4} (-L_s R_r \tilde{i}_{r\alpha} - L_s \tilde{R}_r \hat{i}_{r\alpha} - L_s L_r \omega \tilde{i}_{r\beta} - u_\alpha) \tag{43}$$

$$\dot{\tilde{i}}_{r\beta} = \frac{1}{\gamma_4} (L_s L_r \omega \tilde{i}_{r\alpha} - L_s R_r \tilde{i}_{r\beta} - L_s \tilde{R}_r \hat{i}_{r\beta} - u_\beta) \tag{44}$$

To achieve the design of the rotor resistance identifier the following additive assumption is required.

Assumption (iv) It is assumed that the following rotor resistance identifiability condition holds:

$$|i_{r\alpha}(t)| \geq 0 \quad \text{and} \quad |i_{r\beta}(t)| \geq 0 \quad \forall t \geq 0. \tag{45}$$

By considering the following Lyapunov candidate function

$$V_1 = \frac{1}{2} \tilde{i}_{s\alpha}^2 + \frac{1}{2} \tilde{i}_{s\beta}^2 \tag{46}$$

and computing its time-derivative along the trajectories of (41) and (42), we obtain

$$\begin{aligned} \dot{V}_1 = & \frac{1}{\gamma_4} (L_m L_r \tilde{i}_{r\beta} \tilde{i}_{s\alpha} + L_m R_r \tilde{i}_{r\alpha} \tilde{i}_{s\alpha} + L_m \tilde{R}_r \hat{i}_{r\alpha} \tilde{i}_{s\alpha} \\ & - K |\tilde{i}_{s\alpha}| - L_m L_r \omega \tilde{i}_{r\alpha} \tilde{i}_{s\beta} + L_m R_r \tilde{i}_{r\beta} \tilde{i}_{s\beta} + L_m \tilde{R}_r \\ & \hat{i}_{r\beta} \tilde{i}_{s\beta} - K |\tilde{i}_{s\beta}|) \end{aligned} \tag{47}$$

From (47), by taking into account assumptions (i) and (ii), the following inequalities hold:

$$\begin{aligned} \dot{V}_1 \leq & \frac{1}{\gamma_4} (-|\tilde{i}_{s\alpha}| [K - (L_m L_r \omega |\tilde{i}_{r\beta}| + L_m R_r |\tilde{i}_{r\alpha}| \\ & + L_m \tilde{R}_r |\hat{i}_{r\alpha}|)] - |\tilde{i}_{s\beta}| [K - (L_m L_r \omega |\tilde{i}_{r\alpha}| \\ & + L_m R_r |\tilde{i}_{r\beta}| + L_m \tilde{R}_r |\hat{i}_{r\beta}|)]). \end{aligned} \tag{48}$$

Assuming that the estimate \hat{R}_r , $\hat{i}_{r\alpha}$, and $\hat{i}_{r\beta}$ are bounded,¹ let positive constants ξ_α and ξ_β be available such that

$$\xi_\alpha = \frac{1}{\gamma_4} (L_m L_r \omega |\tilde{i}_{r\beta}|_m + L_m R_r |\tilde{i}_{r\alpha}|_m + L_m \tilde{R}_r |\hat{i}_{r\alpha}|_m) \tag{49}$$

$$\xi_\beta = \frac{1}{\gamma_4} (L_m L_r \omega |\tilde{i}_{r\alpha}|_m + L_m R_r |\tilde{i}_{r\beta}|_m + L_m \tilde{R}_r |\hat{i}_{r\beta}|_m) \tag{50}$$

where $|\cdot|_m$ denotes the maximum value of $|\cdot|$. By choosing

$$K > \sup(\xi_\alpha, \xi_\beta) \tag{51}$$

the derivative of V_1 will be negative definite $\forall \tilde{i}_{s\alpha} \neq 0$ and $\tilde{i}_{s\beta} \neq 0$. Therefore, the observer errors $\tilde{i}_{s\alpha}$ and $\tilde{i}_{s\beta}$ converge to 0 in finite time if the gain K is chosen such that condition (51) is satisfied.

Remark 4 Since the rotor signals are not measurable in the case of squirrel cage induction machine, the gain K in (51) can be selected by trial and error method.

¹ The proof of the boundness will be given later.

We now consider the following quadratic function of the rotor current observer error and rotor resistance estimation error:

$$V_2 = \frac{1}{2}\tilde{i}_{r\alpha}^2 + \frac{1}{2}\tilde{i}_{r\beta}^2 + \frac{1}{2}\tilde{R}_r^2. \tag{52}$$

Its time-derivative along the trajectories of (43) and (44) yields

$$\begin{aligned} \dot{V}_2 = & \frac{1}{\gamma_4}(-L_s R_r \tilde{i}_{r\alpha}^2 - L_s \tilde{R}_r \hat{i}_{r\alpha} \tilde{i}_{r\alpha} - u_\alpha \tilde{i}_{r\alpha} - L_s R_r \tilde{i}_{r\beta}^2 \\ & - L_s \tilde{R}_r \hat{i}_{r\beta} \tilde{i}_{r\beta} - u_\beta \tilde{i}_{r\beta} + \tilde{R}_r \dot{\tilde{R}}_r). \end{aligned} \tag{53}$$

If we choose u_α, u_β and $\dot{\tilde{R}}_r$ as follows (K_{R_r} is a designed parameter):

$$\begin{aligned} u_\alpha &= -L_s \tilde{R}_r \hat{i}_{r\alpha} \\ u_\beta &= -L_s \tilde{R}_r \hat{i}_{r\beta} \\ \dot{\tilde{R}}_r &= \hat{\dot{R}}_r = -K_{R_r} \text{sign}(\tilde{R}_r) \end{aligned} \tag{54}$$

\dot{V}_2 becomes

$$\dot{V}_2 = -\frac{L_s R_r}{\gamma_4}(\tilde{i}_{r\alpha}^2 + \tilde{i}_{r\beta}^2) - K_{R_r} |\tilde{R}_r|. \tag{55}$$

Consequently, under the identifiability condition (45) and if the auxiliary variables u_α, u_β and $\dot{\tilde{R}}_r$ are chosen as in (54), \dot{V}_2 will be negative definite $\forall \tilde{i}_{r\alpha} \neq 0, \forall \tilde{i}_{r\beta} \neq 0$ and $\forall \tilde{R}_r \neq 0$. Thus, $\hat{i}_{r\alpha}, \hat{i}_{r\beta}$ and \hat{R}_r converge in finite time to their nominal values $i_{r\alpha}, i_{r\beta}$ and R_r with the convergence rate $\frac{L_s R_r}{\gamma_4}$ and K_{R_r} , respectively.

Remark 5 If $K_{R_r} > \frac{L_s R_r}{\gamma_4}$, the rotor resistance convergence will be faster than that of the rotor current. In contrary, if $K_{R_r} < \frac{L_s R_r}{\gamma_4}$, the rotor current convergence will be faster than that of the rotor resistance. The case $K_{R_r} = \frac{L_s R_r}{\gamma_4}$ is difficult to implement in practice since R_r is assumed to be unknown and is time-varying but verifies in normal operation of the SEIG $R_{rmin} \leq R_r \leq R_{rmax}$.

To achieve the design of the rotor resistance estimator, implementable expression for \hat{R}_r is required. Under condition (51), a sliding-mode occurs in finite time on the manifold

$$\begin{aligned} \dot{\tilde{i}}_{s\alpha} &= \tilde{i}_{s\alpha} = 0 \\ \dot{\tilde{i}}_{s\beta} &= \tilde{i}_{s\beta} = 0. \end{aligned} \tag{56}$$

The equivalent injection terms [27] can be computed by solving the equation

$$\begin{aligned} \dot{\tilde{i}}_{s\alpha} &= 0 \\ \dot{\tilde{i}}_{s\beta} &= 0. \end{aligned} \tag{57}$$

Consequently, (41) and (42) can be rewritten as

$$\frac{1}{\gamma_4}(L_m L_r \omega \tilde{i}_{r\beta} + L_m R_r \tilde{i}_{r\alpha} + L_m \tilde{R}_r \hat{i}_{r\alpha}) - W_{\alpha eq} = 0 \tag{58}$$

$$\frac{1}{\gamma_4}(-L_m L_r \omega \tilde{i}_{r\alpha} + L_m R_r \tilde{i}_{r\beta} + L_m \tilde{R}_r \hat{i}_{r\beta}) - W_{\beta eq} = 0 \tag{59}$$

where $W_{\alpha eq} = K \text{sign}(\tilde{i}_{s\alpha})$ and $W_{\beta eq} = K \text{sign}(\tilde{i}_{s\beta})$. The expressions of the equivalent injection terms can be deduced from (58) and (59) but these expressions cannot be implemented in practice since $\tilde{i}_{r\alpha}, \tilde{i}_{r\beta}$ and \tilde{R}_r are not available.² To overcome this problem, the equivalent injection terms are approximated using first order low-pass filters as in [27]. If the design parameter K_{R_r} is chosen such that

$$0 < K_{R_r} < \frac{L_s R_{rmin}}{\gamma_4}, \tag{60}$$

the rotor current convergence will be faster than that of the rotor resistance. Under this assumption and identifiability condition (45), the implementable expression of the rotor resistance estimation error \tilde{R}_r can be derived from (58) and (59) by neglecting the terms containing the rotor current estimation error. We then obtain

$$\tilde{R}_r = \frac{\gamma_4(\hat{i}_{r\alpha} W_{\alpha eq} + \hat{i}_{r\beta} W_{\beta eq})}{L_m(\hat{i}_{r\alpha}^2 + \hat{i}_{r\beta}^2)}. \tag{61}$$

Finally, the overall simplified rotor resistance estimator can be summarized as follows:

$$\begin{aligned} \dot{\tilde{i}}_{s\alpha} &= \frac{1}{\gamma_4}(-L_r R_s \tilde{i}_{s\alpha} + L_m^2 \omega \tilde{i}_{s\beta} + L_m \hat{R}_r \hat{i}_{r\alpha} + L_m L_r \omega \hat{i}_{r\beta} \\ &+ L_r v_{s\alpha}) - K \text{sign}(\tilde{i}_{s\alpha}) \\ \dot{\tilde{i}}_{s\beta} &= \frac{1}{\gamma_4}(-L_m^2 \omega \tilde{i}_{s\alpha} - L_r R_s \tilde{i}_{s\beta} - L_m L_r \omega \hat{i}_{r\alpha} \\ &+ L_m \hat{R}_r \hat{i}_{r\beta} + L_r v_{s\beta}) - K \text{sign}(\tilde{i}_{s\beta}) \\ \dot{\tilde{i}}_{r\alpha} &= \frac{1}{\gamma_4}(L_m R_s \tilde{i}_{s\alpha} - L_m L_s \omega \tilde{i}_{s\beta} - L_s \hat{R}_r \hat{i}_{r\alpha} \\ &- L_s L_r \omega \hat{i}_{r\beta} + u_\alpha - L_m v_{s\alpha}) \\ \dot{\tilde{i}}_{r\beta} &= \frac{1}{\gamma_4}(L_m L_s \omega \tilde{i}_{s\alpha} + L_m R_s \tilde{i}_{s\beta} + L_s L_r \omega \hat{i}_{r\alpha} \\ &- L_s \hat{R}_r \hat{i}_{r\beta} + u_\beta - L_m v_{s\beta}) \end{aligned}$$

² R_r is assumed to be unknown and $i_{r\alpha}$ and $i_{r\beta}$ are not measurable.

$$u_\alpha = -L_s \tilde{R}_r \hat{i}_{r\alpha}, \quad u_\beta = -L_s \tilde{R}_r \hat{i}_{r\beta}$$

$$\dot{\hat{R}}_r = -K_{R_r} \text{sign}(\tilde{R}_r) \text{ with } \tilde{R}_r = \frac{\gamma_4(\hat{i}_{r\alpha} W_{\alpha eq} + \hat{i}_{r\beta} W_{\beta eq})}{L_m(\hat{i}_{r\alpha}^2 + \hat{i}_{r\beta}^2)} \quad (62)$$

3.4.2 Rotor flux and stator electrical angular position estimation algorithms

Rotor flux observer design

Let us now consider the following observer for ϕ_r

$$\dot{\hat{\phi}}_r = \frac{L_m \hat{R}_r}{L_r} i_{sd} - \frac{\hat{R}_r}{L_r} \hat{\phi}_r \quad (63)$$

and let $\tilde{\phi}_r = \phi_r - \hat{\phi}_r$ be the rotor flux observer error. By taking into account (8), the observer error dynamic equation may be computed as follows:

$$\dot{\tilde{\phi}}_r = \frac{\tilde{R}_r}{L_r} (L_m i_{sd} - \phi_r) - \frac{\hat{R}_r}{L_r} \tilde{\phi}_r \quad (64)$$

From the fact that \tilde{R}_r converges to the neighborhood of 0 in finite time, the observer error $\tilde{\phi}_r$ converges to the neighborhood of 0 which immediately implies that $\hat{\phi}_r$ converges to ϕ_r .

Stator electrical angular position estimation algorithm

Assuming that the estimates of the rotor resistance and rotor flux converge in finite time to their nominal values, the estimation of the stator electrical angular position can be achieved by using (9) as follows.

$$\hat{\omega}_s = \omega + \frac{L_m \hat{R}_r}{L_r} \frac{i_{sq}}{\hat{\phi}_r}, \quad \hat{\theta}_s = \int \hat{\omega}_s dt + \hat{\theta}_s(0) \quad (65)$$

Remark 6 The proposed adaptive nonlinear control is not a direct current control. To limit the reference value of v_{sd} and v_{sq} (which implicitly limits the current reference value), saturated functions have been used. However, in the practice, the SEIG based system should be equipped with a fast over current protection unit.

3.5 Global convergence and stability analysis

To achieve the global convergence and stability analysis, let us recall the non-adaptive nonlinear controller (22)–(23):

$$v_{sd} = v_{sdeq} - k_{v_{sd}} \text{sign}(s_{\phi_r}) \quad (66)$$

$$v_{sq} = v_{sqeq} - k_{v_{sq}} \text{sign}(s_{\omega_m}) \quad (67)$$

where

$$v_{sdeq} = \frac{1}{a_4} \left[f_{\phi_r} - \ddot{\phi}_r^* - c_{\phi_r} \dot{\phi}_r^* + c_{\phi_r} \left(\frac{L_m}{\tau_r} i_{sd} - \frac{1}{\tau_r} \phi_r \right) \right], \quad (68)$$

$$v_{sqeq} = -\frac{1}{b_9} [f_{\omega_m} + c_{\omega_m} (k_{opt} \omega_m^2 - \frac{n_p L_m}{L_r} \phi_r i_{sq} - f \omega_m)] \quad (69)$$

Note that it has been proved in section 3.3 that the above non-adaptive controller achieves finite time convergence of the tracking errors to zero of the rotor speed and rotor flux of SEIG associated to PWM converter.

In practice, the adaptive controller is used because the rotor flux ϕ_r is not measurable and the observer of the rotor flux depends up-on the rotor resistance R_r which is assumed to be unknown time-varying parameter. In addition, the equivalent terms (68)–(69) and the stator electrical angular position θ_s require the knowledge of the rotor flux and rotor resistance. In this case, θ_s , R_r and ϕ_r are substituted in the above non-adaptive controller by their estimates.

The global convergence and stability analysis taking into account the interconnections between R_r , ϕ_r and θ_s estimators and the nonlinear controller are based on the separation principle theorem. The finite-time convergence of the estimation algorithms allows to design the estimators and the nonlinear control law separately, i.e., the separation principle is satisfied [29,30]. The only requirement for its implementation is the boundedness of the states of the system [assumptions (i)–(iii), the identifiability condition (45), conditions (51) and (60)] in the operational domain.

3.6 DC-link voltage control strategy design

In order to regulate the dc-link voltage, an electronic load controller (ELC) is proposed. This ELC consists of an insulated gate bipolar transistor IGBT operating as a chopper connected in series with a dump load resistance R_L . This dump load is designed such that when the duty cycle of the chopper is unity (during fault or over-generation), it should consume the maximum output power of the generator. The dump load can be a heater load or a battery charging load. Using the power balance principle, the dynamic behavior of the dc-bus voltage is given by [31]

$$\frac{C}{2} \frac{dv_{dc}^2}{dt} = \omega_m T_e - \frac{Sv_{dc}^2}{R_L} - P_{in} \quad (70)$$

where P_{in} is the input power of the inverter. We rewrite (70) as follows.

$$\frac{dv_{dc}}{dt} = f_{v_{dc}} + g_{v_{dc}} v_{\alpha}, \text{ with } v_{\alpha} = S v_{dc} \tag{71}$$

$$f_{v_{dc}} = \frac{\omega_m T_e}{C v_{dc}} - \frac{P_{in}}{C v_{dc}}, \text{ and } g_{v_{dc}} = -\frac{1}{R_L C}. \tag{72}$$

The expression for the DC-link voltage control of v_{dc} can be easily computed as in the case of ϕ_r and ω_m control strategy (Sect. 3.3) as follows

$$v_{\alpha}^* = -\frac{1}{g_{dc}}(f_{dc} + k_{i_{dc}} e_{dc}) - k_{p_{dc}} \text{sign}(S_{dc}),$$

where $S_{dc} = e_{dc} + k_{i_{dc}} \int e_{dc}, \quad e_{dc} = v_{dc} - v_{dc}^*.$

$$\tag{73}$$

4 Load side inverter control strategy design

The control objective in the load side inverter is the regulation of the AC load voltage magnitude. Note that the frequency of the load voltages and currents is imposed by the frequency of the load ω_e used in the (a, b, c) coordinate frame $\rightarrow (d, q)$ coordinate frame transformation.

4.1 Modeling of voltage source inverter and LC filter

The voltage source inverter is connected to the AC load through an LC filter. In the synchronously rotating reference frame d and q axis, the voltage equations are given by [31]:

$$\dot{i}_{id} = -\frac{R_f}{L_f} i_{id} + \omega_e i_{iq} + \frac{1}{L_f} v_{id} - \frac{1}{L_f} v_d \tag{74}$$

$$\dot{i}_{iq} = -\frac{R_f}{L_f} i_{iq} - \omega_e i_{id} + \frac{1}{L_f} v_{iq} - \frac{1}{L_f} v_q \tag{75}$$

$$\dot{v}_d = \frac{1}{C_f} i_{id} - \frac{1}{C_f} i_{Ld} \tag{76}$$

$$\dot{v}_q = \frac{1}{C_f} i_{iq} - \frac{1}{C_f} i_{Lq} \tag{77}$$

The notation for the above nonlinear dynamics is given in ‘‘Appendix 7’’. The methodology used to obtain the filter parameters is described in [32] and is given in ‘‘Appendix 8’’.

Assuming that the load side inverter currents in the synchronously rotating reference frame d and q axis are constants, the equations used for the derivation of the control law in this section can be computed using the differentiation of (76) and (77) combined with (74) and (75). This leads to:

$$\ddot{v}_d = \frac{1}{C_f} \left(-\frac{R_f}{L_f} i_{id} + \omega_e i_{iq} + \frac{1}{L_f} v_{id} - \frac{1}{L_f} v_d \right) \tag{78}$$

$$\ddot{v}_q = \frac{1}{C_f} \left(-\frac{R_f}{L_f} i_{iq} - \omega_e i_{id} + \frac{1}{L_f} v_{iq} - \frac{1}{L_f} v_q \right) \tag{79}$$

Assuming that the load side voltage reference values in the synchronously rotating reference frame d and q axis are constants, the expressions for the load side inverter control of v_d and v_q can be easily computed as in the case of ϕ_r and ω_m control strategy (Sect. 3.3) as follows

$$v_{id}^* = v_{ideq} - k_{v_{id}} \text{sign}(s_{v_d}) \tag{80}$$

$$v_{iq}^* = v_{iqeq} - k_{v_{iq}} \text{sign}(s_{v_q}) \tag{81}$$

where

$$v_{ideq} = (R_f - L_f C_{v_d}) i_{id} - \omega_e L_f i_{iq} + v_d + L_f C_{v_d} i_{Ld}, \quad s_{v_d} = \left(\frac{d}{dt} + C_{v_d} \right) (v_d - v_d^*) \tag{82}$$

$$v_{iqeq} = (R_f - L_f C_{v_q}) i_{iq} + \omega_e L_f i_{id} + v_q + L_f C_{v_q} i_{Lq}, \quad s_{v_q} = \left(\frac{d}{dt} + C_{v_q} \right) (v_q - v_q^*). \tag{83}$$

Remark 7 To reduce the chattering phenomenon on the proposed controllers, the sign function has been approximated as [33]

$$\text{sign}(\cdot) = \frac{(\cdot)}{|\cdot| + \epsilon} \text{ with } 0 < \epsilon < 1. \tag{84}$$

The structure of the proposed nonlinear controllers is depicted in Fig. 2.

4.2 Controller parameters tuning

It is worth observing that, in order to increase the tracking performance of the above controllers, a rigorous methodology for the optimal tuning of the controller design parameters is required. However, it is difficult to define such a methodology, since the overall adaptive control is nonlinear with time-varying adaptive parameters. In this section, some guidelines for the selection of controller parameter values (i.e. $c_{\omega_m}, c_{\phi_r}, k_{v_{sq}}, k_{v_{sd}}$ in Sect. 3.3) are given.

The following considerations have to be taken into account.

- c_{ω_m} and c_{ϕ_r} should be chosen sufficiently smaller than the frequency (in rad/s) of the lowest unmodeled dynamics.
- the larger $c_{\omega_m}, c_{\phi_r}, k_{v_{sq}}$ and $k_{v_{sd}}$, the worse the effect of noise present in the input of the adaptive controller;
- in real-time implementation using DSP, c_{ω_m} and c_{ϕ_r} should be chosen sufficiently smaller than the sampling frequency (in rad/s).

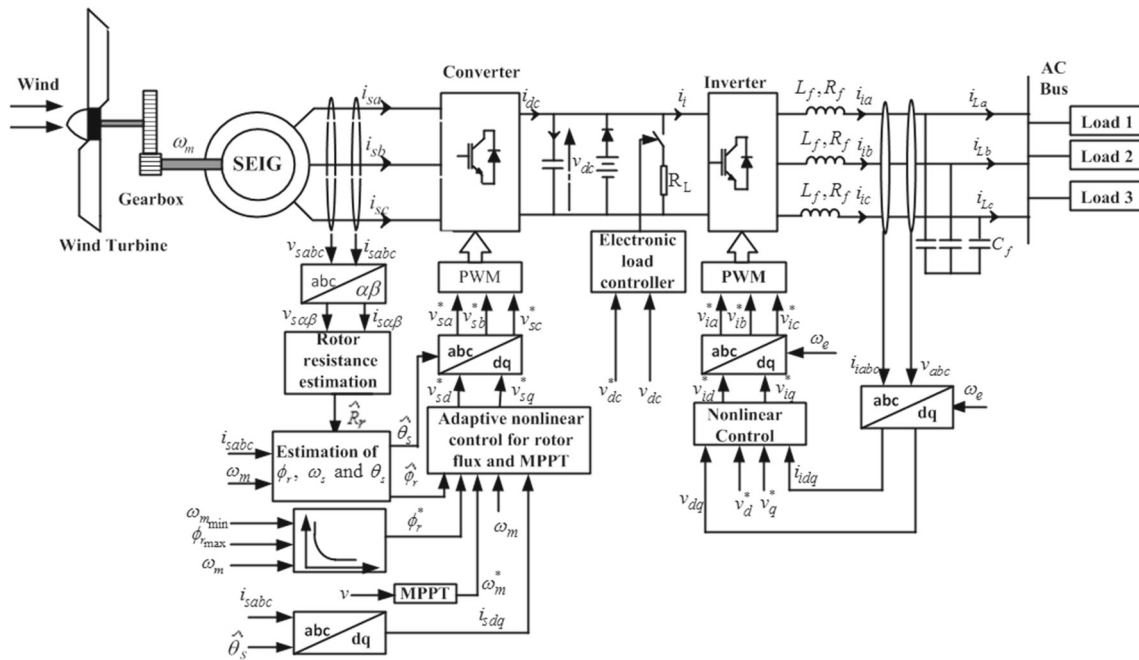


Fig. 2 Structure of the proposed adaptive nonlinear controllers

Hence the values of c_{ω_m} , c_{ϕ_r} , $k_{v_{sq}}$ and $k_{v_{sd}}$ should be chosen using the above guidelines in order to obtain a trade-off between the signal content preservation and the noise reduction.

5 Simulation results

The effectiveness of the proposed nonlinear controller (NC) has been verified by numerical simulations within the Matlab/Simulink environment software with sampling time of $40\mu s$. This sampling time is real-time implementable using actual commercial DSP1104 [34]. The parameters of the induction machine, generator side converter and load side inverter used in the simulation are given in “Appendices 1, 2 and 3”, respectively.

Two sets of simulation have been performed. For comparison, these simulations have been performed using both nonlinear controllers and conventional P.I regulators. The structures of the P.I regulators are given in Figs. 3 and 4.

In all simulations, the capacitive load RC , inductive load RL , and the RLC load have been applied at time $t = 0s$, $t = 1.5s$ and $2.5s$, respectively. The values of the different loads have been chosen as follows.

Capacitive load RC : $R = 150\Omega$, $C = 30mF$. Inductive load RC : $R = 150\Omega$, $L = 50mH$. Combined inductive-capacitive load RLC : $R = 150\Omega$, $L = 50mH$, $C = 30mF$. The frequency of the load is $\omega_e = 100\pi$.

The tuning parameters of the nonlinear controllers selected according to the procedure described in Sect. 4.2, have been chosen as follows.

Rotor flux magnitude and rotor speed controllers gains: $c_{\omega_m} = 200$, $k_{v_{sq}} = 30$, $c_{\phi_r} = 300$ and $k_{v_{sd}} = 50$. DC-link voltage regulation gains: $k_{i_{dc}} = 2$ and $k_{p_{dc}} = 10$.

Load side inverter nonlinear controllers gains: $c_{v_d} = 10$, $k_{v_d} = 10$, $c_{v_q} = 20$ and $k_{v_q} = 10$. The gains of the rotor resistance identifier are $K = 50$ and $K_{R_r} = 35$. The equivalent injection terms have been approximated using first order low-pass filter with time-constant of $3.5ms$ and the sign function in the controller (66)–(67) has been approximated using (84) with $\epsilon = 0.01$. Note that the value of K_{R_r} verifies condition (60) since $\frac{L_s R_{rmin}}{L} = 128.2s^{-1}$. The initial value of θ_s is $0.01rad$. The parameters of the LC filter used in the load side inverter are: $L_f = 40mH$, $C_f = 10\mu F$ and $R_f = 0.1\Omega$.

The tuning parameters of the PI regulators selected according to the procedure described in “Appendix 5”, have been chosen as follows.

Generator converter side

Rotor flux regulator: $k_{p_{\phi_r}} = 110$, $k_{i_{\phi_r}} = 1660$.
 Rotor speed regulator: $k_{p_{\omega_m}} = 4$, $k_{i_{\omega_m}} = 1$.
 Stator current components i_{sd} and i_{sq} regulators: $k_{p_{i_{sd}}} = k_{p_{i_{sq}}} = 100$, $k_{i_{i_{sd}}} = k_{i_{i_{sq}}} = 600$.

Grid inverter side

Load voltage direct axis component PI regulators gains: $k_{p_{v_d}} = 0.45$, $k_{i_{v_d}} = 1.2$, $k_{p_{i_d}} = 10$ and $k_{i_{i_d}} = 5$.

Fig. 3 Structure of the PI regulators in the generator side

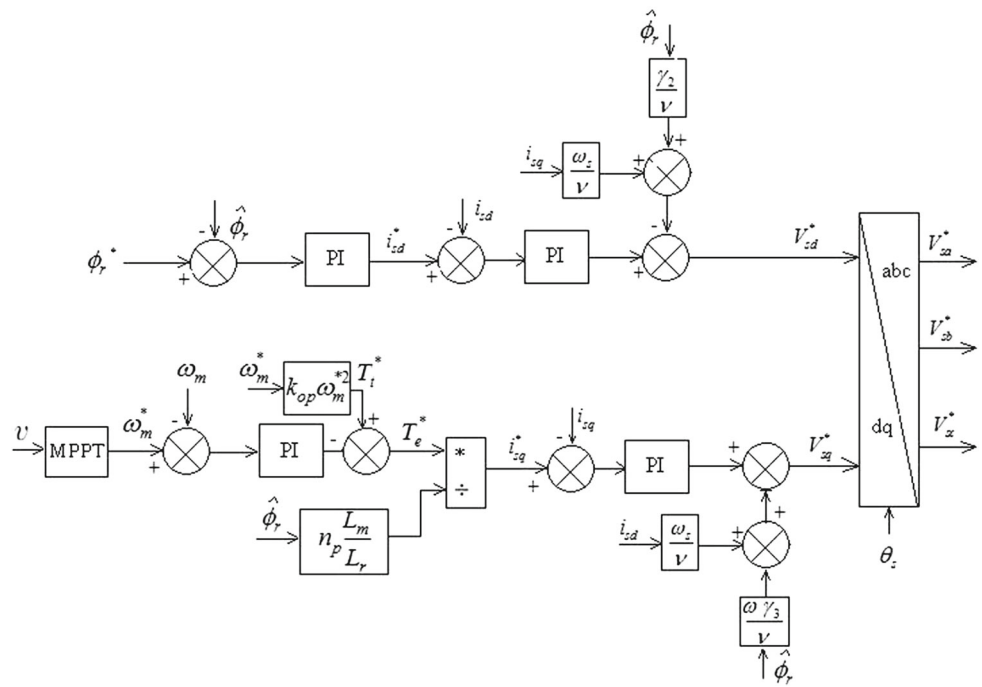
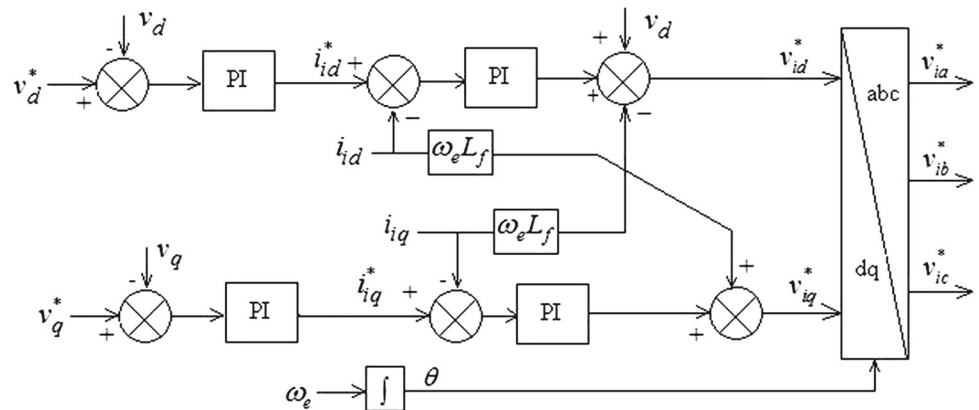


Fig. 4 Structure of the PI regulators in the load side



Load voltage quadrature axis component PI regulators gains: $k_{pv_q} = 10$, $k_{iv_q} = 5$, $k_{pi_q} = 5$ and $k_{ii_q} = 2.5$.

To verify the effectiveness and robustness of the proposed method, all simulations have been carried out with SEIG driven by variable wind speed turbine and under noise condition when the magnitude of the noise reaches about 3.75% of the maximum values of the measurable stator currents (Figs. 5, 6, 7, 8, 9, 10, 11, 12, 13, 14).

In the first set of simulation, the stator resistance is assumed to be constant while the rotor resistance is assumed to be time-varying. This variation starts at time $t = 1$ s and reaches 100% of the nominal value of R_r at time $t = 2$ s. The results are depicted in Figs. 5, 6, 7, 8, 9 and 10.

It can be noticed from these figures the good performance of the proposed nonlinear control and the poor performance of the P.I regulators under online variation of

the rotor resistance and when the wind speed varies from 9 to 6.5 m/s at time $t = 3.5$ s. The steady state errors obtained when the wind speed varies from 9 to 6.5 m/s at time $t = 3.5$ s show that the results obtained using the nonlinear controller are more precise than those provided by PI regulators. During transient periods, the performance obtained using PI regulators exhibits higher overshoot values than the performance provided by the nonlinear controllers (Figs. 9b, 14b). One can also notice that the convergence times of the rotor current and rotor resistance are 0.015, and 0.14 s, respectively. Thus the assumption that the rotor current convergence must be faster than the convergence time of the rotor resistance is satisfied. Under load variations, both controllers provided good performance as shown in Figs. 6b and 12b. One can also notice that the control signal value in the case of the PI regulators is greater than the

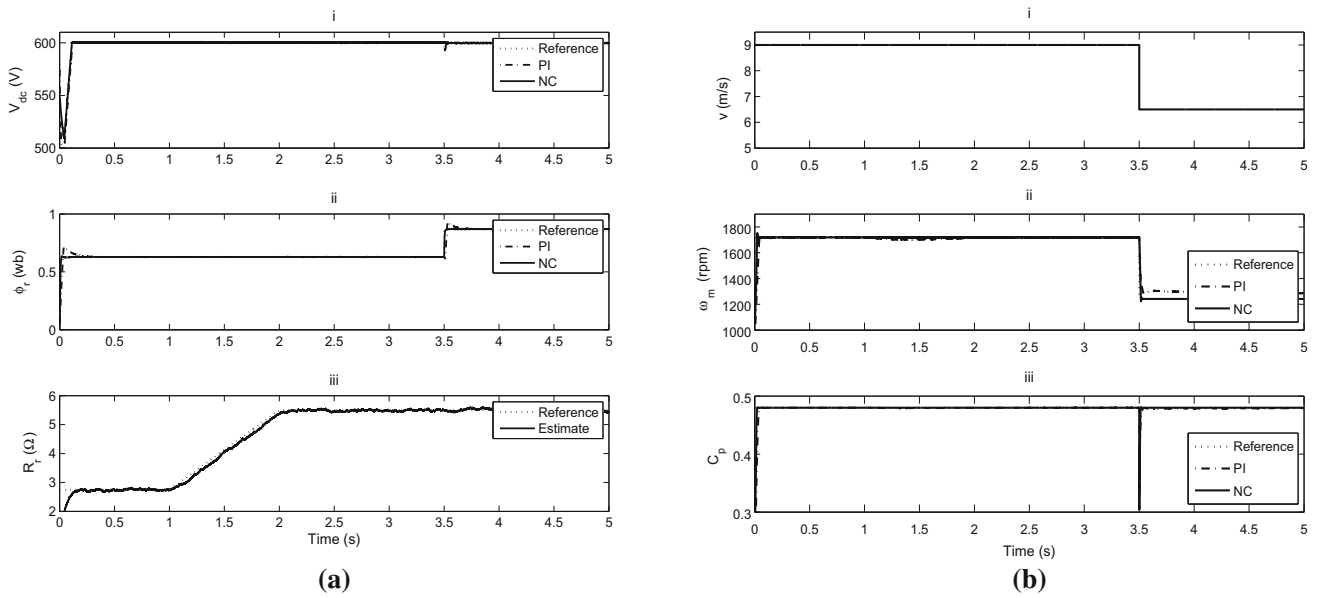


Fig. 5 First set of simulation: Comparative performances when the stator resistance is assumed to be constant under online variation of the rotor resistance (variation starts at time $t = 1$ s and reaches 100% at

time $t = 2$ s). **a** DC-bus voltage (i), rotor flux magnitude (ii), and rotor resistance (iii). **b** Wind speed (i), rotor speed (ii), and power coefficient (iii)

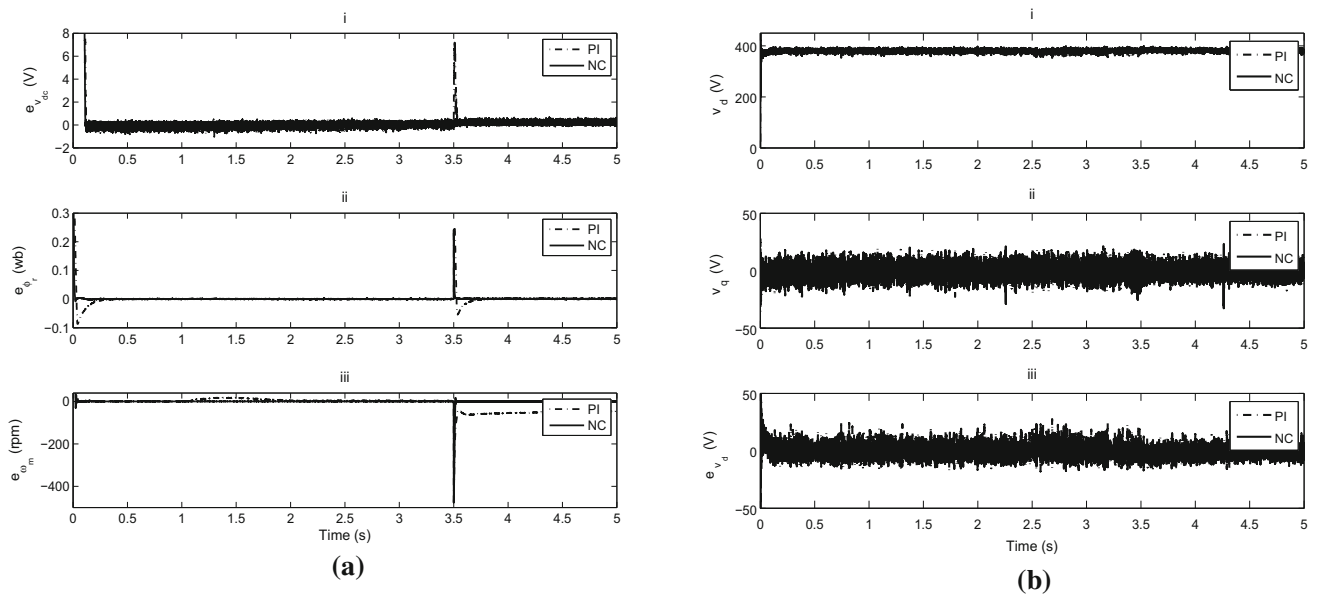


Fig. 6 First set of simulation: Comparative performances when the stator resistance is assumed to be constant under online variation of the rotor resistance (variation starts at time $t = 1$ s and reaches 100% at time $t = 2$ s). **a** DC-bus voltage regulation error (i), rotor flux magni-

tude tracking error (ii) and rotor speed tracking error (iii). **b** d -axis load voltage component (i), and q -axis load voltage component (ii), d -axis load voltage component regulation error (iii)

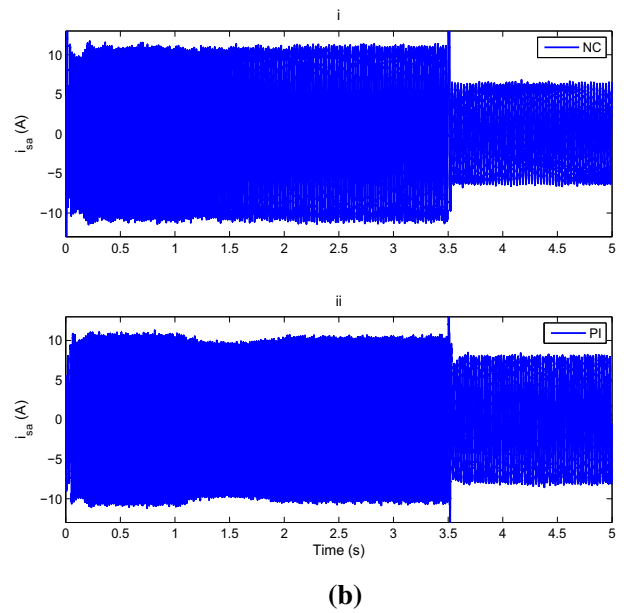
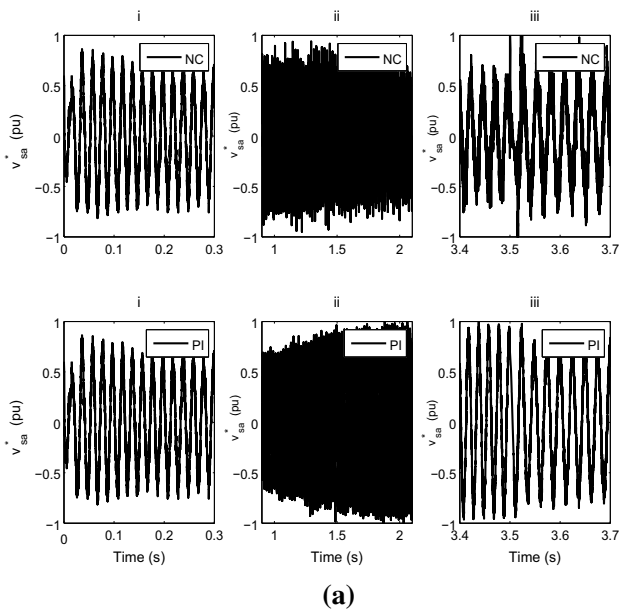


Fig. 7 First set of simulation: Performance when the stator resistance is assumed to be constant under online variation of the rotor resistance (variation starts at time $t = 1$ s and reaches 100% at time $t = 2$ s). **a** Control signal during transient periods in the case of the NC (*i*, *ii* and *iii*). **b** SEIG stator current component i_{sa} in the case of the NC (*i*); SEIG stator current component i_{sa} in the case of the PI regulator (*ii*)

iii); control signal during transient periods in the case of the PI regulator (*i*, *ii* and *iii*). **b** SEIG stator current component i_{sa} in the case of the NC (*i*); SEIG stator current component i_{sa} in the case of the PI regulator (*ii*)

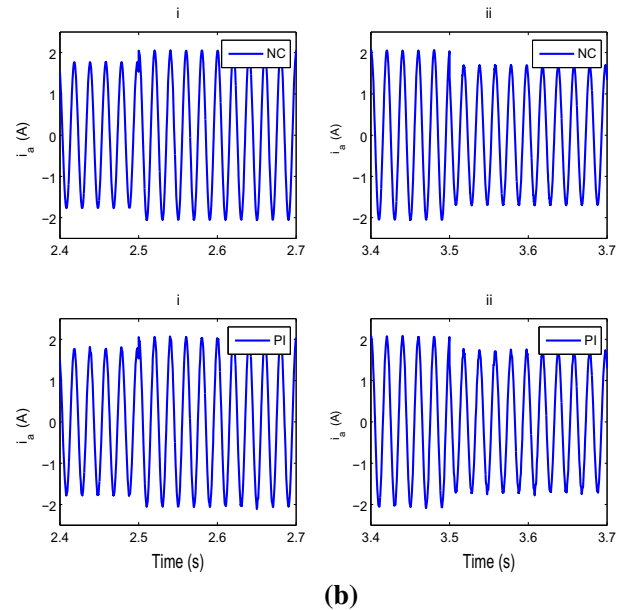
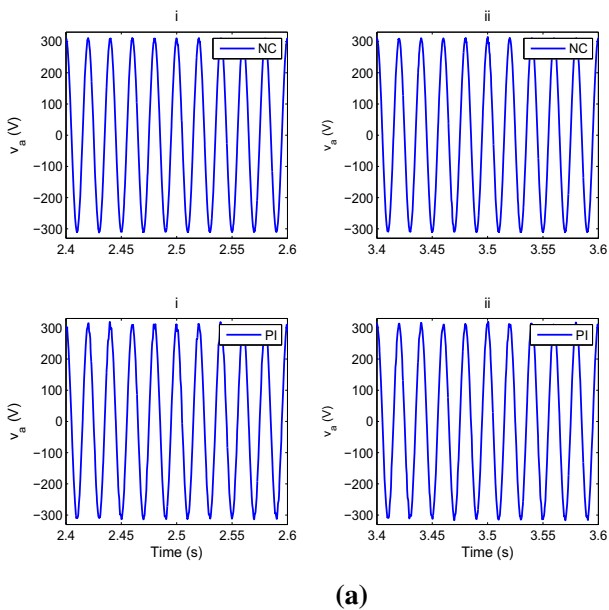


Fig. 8 First set of simulation: Performance when the stator resistance is assumed to be constant under online variation of the rotor resistance (variation starts at time $t = 1$ s and reaches 100% at time $t = 2$ s). **a** Load voltage component v_a during transient periods in the case of the

NC (*i* and *ii*); load voltage component v_a during transient periods in the case of the PI regulator (*i* and *ii*). **b** Load current component i_a during transient periods in the case of the NC (*i* and *ii*); load current component i_a during transient periods in the case of the PI regulator (*i* and *ii*)

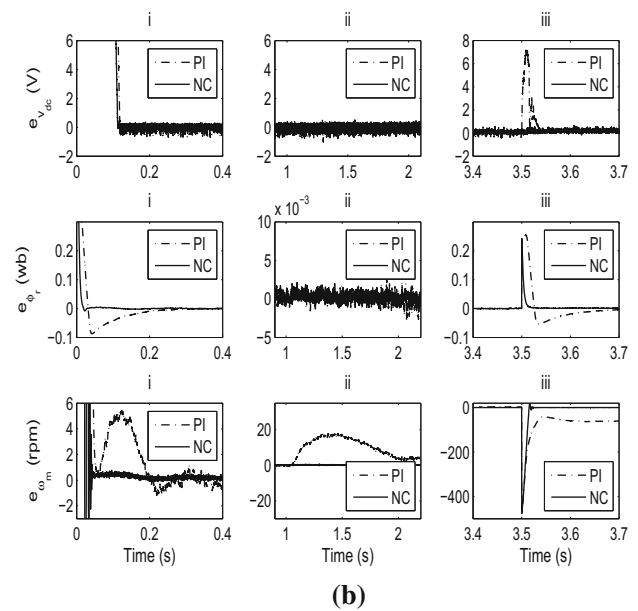
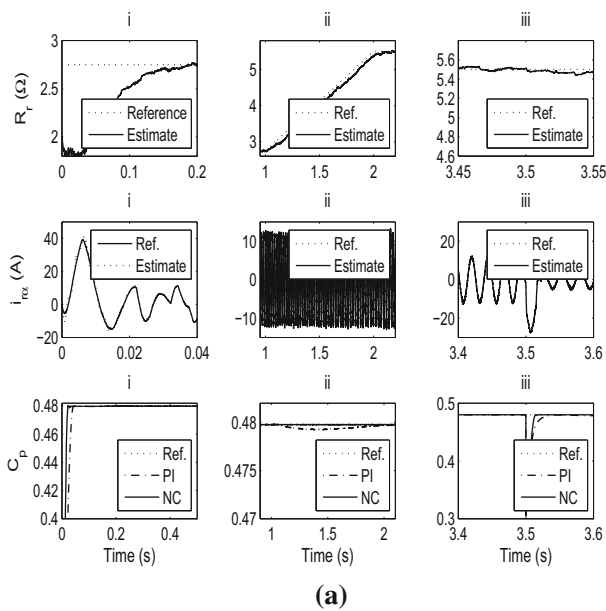


Fig. 9 First set of simulation: Performance when the stator resistance is assumed to be constant under online variation of the rotor resistance (variation starts at time $t = 1$ s and reaches 100% at time $t = 2$ s). **a**

Zoom in Fig. 5a, iii for R_r , zoom of the rotor current component $\hat{i}_{r\alpha}$ and zoom in Fig. 5b, iii for C_p during transient periods. **b** Zoom in Fig. 6a

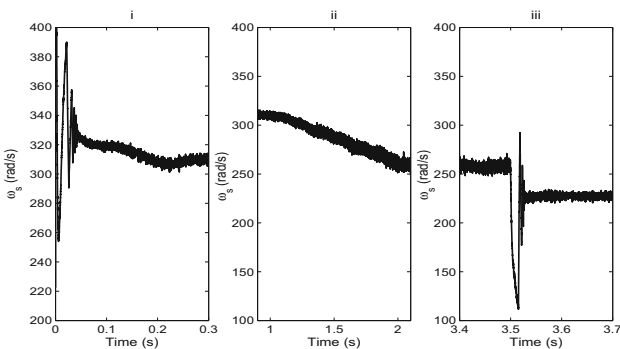


Fig. 10 First set of simulation: Performance when the stator resistance is assumed to be constant under online variation of the rotor resistance (variation starts at time $t = 1$ s and reaches 100% at time $t = 2$ s). Estimate of the electrical angular frequency ω_s during transient (*i*, *ii* and *iii*) required for the implementation of both nonlinear control and PI regulators in the generator side

value obtained in the case of the adaptive nonlinear control when rotor resistance variation occurs at time $t = 1$ s and when the wind speed varies from 9 to 6.5 m/s at time $t = 3.5$ s.

In the second set of simulation, the performance of both controllers under 50% variation of the stator resistance (this variation occurs at time $t = 2.5$ s) has been investigated while the rotor resistance is assumed to be time-varying as in the

first set of simulation. In this case, the obtained results are shown in Figs. 11, 12, 13 and 14.

The remarks made for the previous case are also valid for the present case. It can be noticed the robustness of both controllers with respect to stator resistance variation.

The convergence times of the estimation of the rotor current component, the rotor resistance, rotor flux, stator angular position (via the electrical angular frequency ω_s) and the convergence time of the rotor speed and dc-link voltage have been estimated during the start-up period of the control system in the generator side and are given in Table 1 (all these convergence times are taken from the initial start-up time $t_0 = 0$). From this table, one can notice that the convergence time of the rotor speed (0.04 s) is less than the convergence time of the rotor resistance (0.14 s) due to the robustness of the proposed control with respect to parameter uncertainties. The convergence time of the proposed control algorithm is the maximum convergence time of the control outputs (convergence time of the dc-link voltage: 0.11 s).

Finally, the comparative results show globally that the nonlinear control algorithm provided better performance than the P.I regulators in the generator side control strategy while in the load side inverter control strategy, both nonlinear controller and P.I regulators achieved satisfactorily performance.

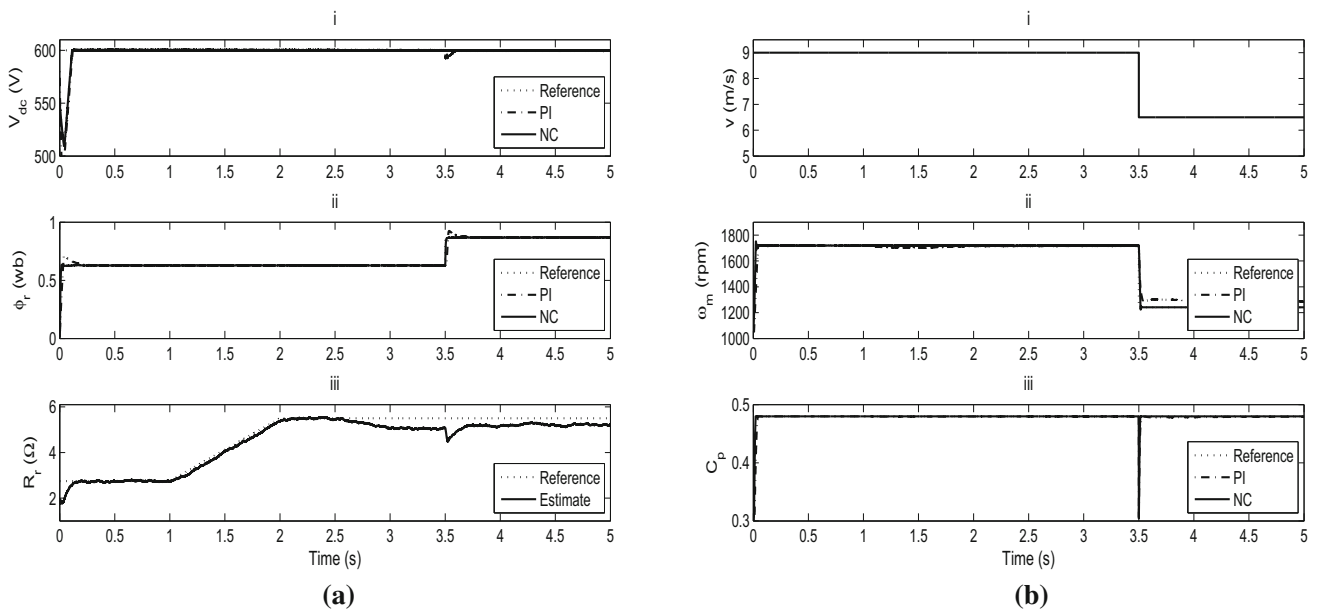


Fig. 11 Second set of simulation: Comparative performances under online variation of the rotor resistance (variation starts at time $t = 1$ s and reaches 100% at time $t = 2$ s) and 50% stator resistance variation

at $t = 2.5$ s. **a** DC-bus voltage (i), rotor flux magnitude (ii), and rotor resistance (iii). **b** Wind speed (i), rotor speed (ii), and power coefficient (iii)

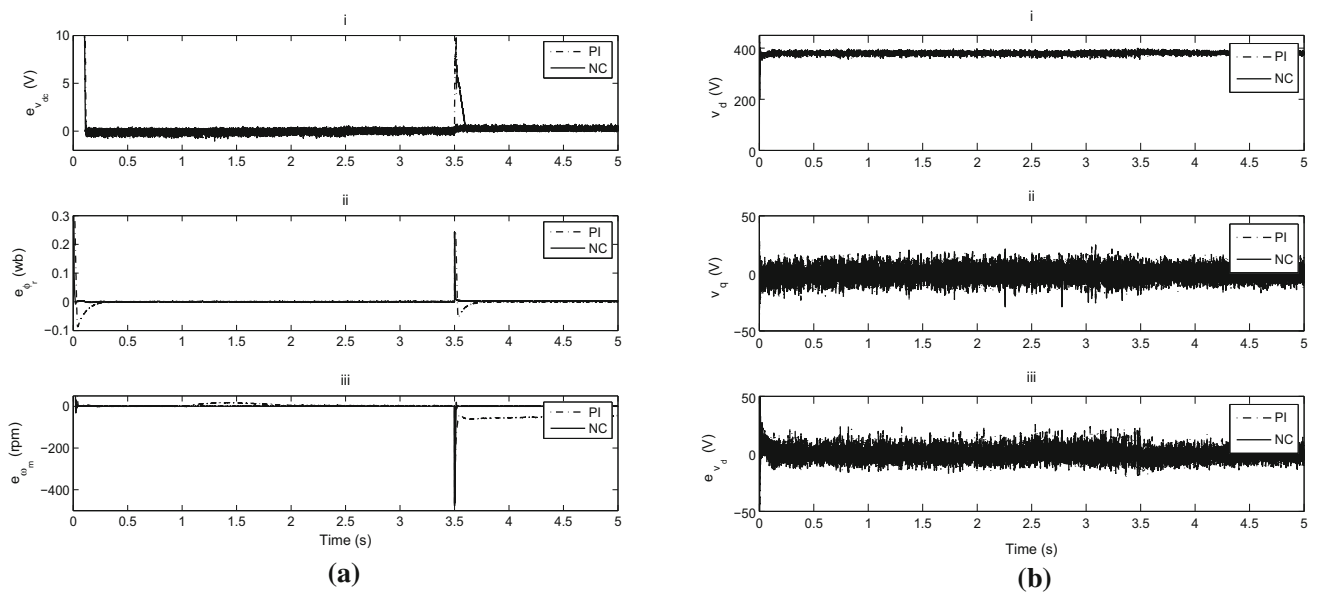


Fig. 12 Second set of simulation: Comparative performances under online variation of the rotor resistance (variation starts at time $t = 1$ s and reaches 100% at time $t = 2$ s) and 50% stator resistance variation at $t = 2.5$ s. **a** DC-bus voltage regulation error (i), rotor flux magnitude

tracking error (ii) and rotor speed tracking error (iii). **b** d-axis load voltage component (i), and q-axis load voltage component (ii), load voltage magnitude regulation error (iii)

6 Conclusion

In this paper, a new control strategy of a stand-alone variable speed based SEIG wind energy conversion has been investigated. Maximum extraction of available energy from

the wind turbine and regulation of the rotor flux magnitude and DC-link voltage in the generator side as well as the regulation of the load voltage magnitude in the inverter load side under wind speed, load and rotor/stator resistances variations have been achieved using adaptive

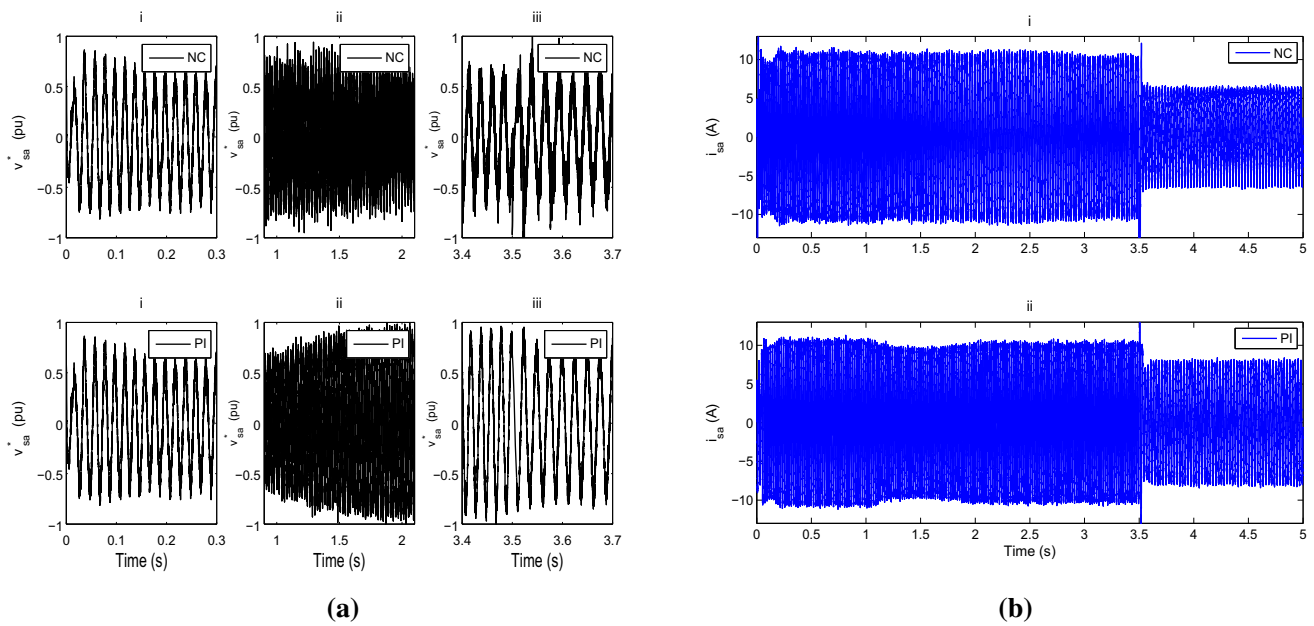


Fig. 13 Second set of simulation: Comparative performances under online variation of the rotor resistance (variation starts at time $t = 1$ s and reaches 100% at time $t = 2$ s) and 50% stator resistance variation at $t = 2.5$ s. **a** Control signal during transient periods in the case of the

NC (*i, ii and iii*); Control signal during transient periods in the case of the PI regulator (*i, ii and iii*). **b** SEIG stator current component i_{sa} in the case of the NC (*i*); SEIG stator current component i_{sa} in the case of the PI regulator (*ii*)

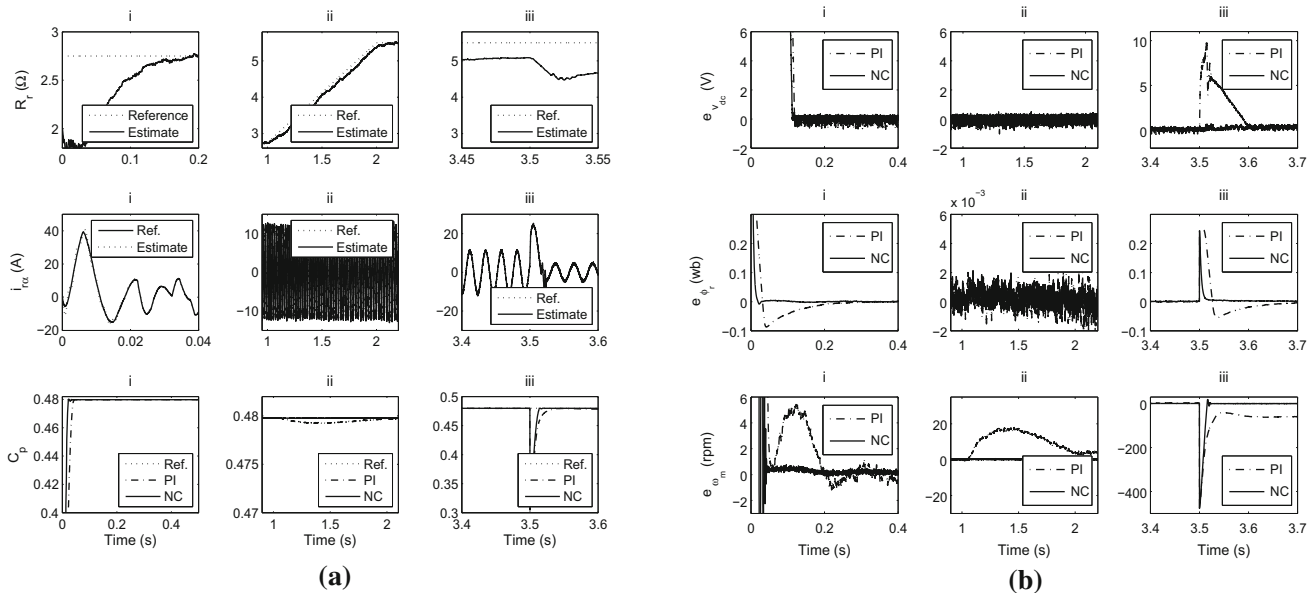


Fig. 14 Second set of simulation: Comparative performances under online variation of the rotor resistance (variation starts at time $t = 1$ s and reaches 100% at time $t = 2$ s) and 50% stator resistance variation

at $t = 2.5$ s. **a** Zoom in Fig. 11a, iii for R_r , zoom of the rotor current component $\hat{i}_{r\alpha}$ and zoom in Fig. 11b, iii for C_p during transient periods. **b** Zoom in Fig. 6a

nonlinear controller and PI regulators. Comparative results show globally that the nonlinear control algorithm provided better performance than the P.I regulators in the generator side control strategy while both nonlinear controller and P.I regulators achieved satisfactorily performance in

the load side inverter control strategy. Finally, the proposed stand-alone variable speed based SEIG wind energy conversion systems can be used in remote and isolated areas where the mean value of the wind speed profile is relatively low.

Table 1 Convergence times for R_r , Φ_r , ω_s and ω_m during the start-up period of the control system in the generator side

| Variable/parameter | $i_{r\alpha}$ | R_r | Φ_r | ω_s | ω_m | v_{dc} |
|----------------------|---------------|-------|----------|------------|------------|----------|
| Convergence time (s) | 0.015 | 0.14 | 0.02 | 0.04 | 0.04 | 0.11 |

Appendix 1: Induction machine parameters [19]

Power: 3.5 kw; Rated speed: 1450 rpm; Rated field current: 7.8 A; $n_p = 2$; $L_r = L_s = 191.4$ mH; $L_m = 180$ mH; $R_s = 1.66 \Omega$; $R_r = 2.75 \Omega$.

Appendix 2: Parameters of the generator side converter

Switching frequency: 6 kHz; DC link capacitor: 2000 μ F

Appendix 3: Parameters of the load side inverter

Switching frequency: 6 kHz; $R_f = 0.1 \Omega$, $C_f = 10 \mu$ F and $L_f = 40$ mH.

Appendix 4: Wind turbine characteristics

Density of air $\rho = 1.225$, Area swept by blades, $A = 19.635$ m², Optimum coefficient, $k_{op} = 0.0037$ Nm/(rad/s)², $C_{pmax} = 0.48$, Cut-in wind speed $v_{min} = 3.5$ m/s, Cut-out wind speed $v_{max} = 25$ m/s, Gearbox ratio $n_g = \frac{\omega_m}{\omega_{mt}} = 6.25$, Turbine total inertia, $J_t = 3$ kg m², Turbine total external damping, $f = 0.0027$ Nm/(rad/s).

Appendix 5: Method for the determination of PI controller parameters

Design of the rotor flux PI regulators

The open loop transfer function of the subsystem described by (8) is given by:

$$\frac{\varphi_r(s)}{i_{sd}(s)} = \frac{\frac{L_m R_r}{L_r}}{s + \frac{R_r}{L_r}} \tag{85}$$

where $s = d/dt$ is the Laplace operator.

Two PI regulators are required to regulate the rotor flux. The first regulator provides the reference stator current component i_{sd}^* while the second one is used for the control of the stator current component i_{sd} . Let us denote $C_{\phi_r}(s)$ the transfer function of the first PI regulator. Its expression is:

$$C_{\phi_r}(s) = \frac{k_{p\phi_r} \left(\frac{k_{i\phi_r}}{k_{p\phi_r}} + s \right)}{s} \tag{86}$$

where $k_{p\phi_r}$ and $k_{i\phi_r}$ are positive tuning gains. The open loop transfer function $G_{OC_{\phi_r}}(s)$ taking into account the PI regulator is:

$$G_{OC_{\phi_r}}(s) = \frac{k_{p\phi_r} L_m R_r}{L_r} \times \frac{\frac{k_{i\phi_r}}{k_{p\phi_r}} + s}{s \left(s + \frac{R_r}{L_r} \right)} \tag{87}$$

The compensation of the pole of $G_{OC_{\phi_r}}(s)$ by the zero of the PI regulator yields

$$\frac{k_{i\phi_r}}{k_{p\phi_r}} = \frac{R_r}{L_r} \tag{88}$$

$$\text{and } G_{OC_{\phi_r}}(s) = \frac{L_m k_{p\phi_r} R_r}{L_r s} \tag{89}$$

The closed-loop transfer function $F_{OC_{\phi_r}}(s)$ can be computed as:

$$F_{OC_{\phi_r}}(s) = \frac{1}{\frac{L_r}{R_r L_m k_{p\phi_r}} s + 1} \tag{90}$$

The above closed-loop transfer function represents a standard first-order system with time-constant $\tau_{\phi_r} = \frac{L_r}{R_r L_m k_{p\phi_r}}$.

It is well known that after three time constants, the first-order unit step response is within 95 percent of its steady state value. Thus the settling time $t_{S(5\%)}$ typically defined to be the time at which the response enters and remains within a ± 5 percent band about the steady-state value can be approximated in the case of first-order system by

$$t_{S_{\phi_r}(5\%)} = 3\tau_{\phi_r} \tag{91}$$

Consequently, given a desired settling time $t_{S_{\phi_r}(5\%)}$, from (88) and (91), we can deduce the expressions for $k_{p\phi_r}$ and $k_{i\phi_r}$ as:

$$k_{p\phi_r} = \frac{3L_r}{R_r L_m t_{S_{\phi_r}(5\%)}} \tag{92}$$

$$k_{i\phi_r} = \frac{3}{L_m t_{S_{\phi_r}(5\%)}} \tag{93}$$

The same procedure can be applied to design the second PI regulator for the rotor flux control loop and others PI regulators used in this work.

Appendix 6: Relation between the nominal value v_{dcn} and the nominal line-to-line RMS supply voltage $v_{n_{sac}}$

This relation is given by [35]:

$$v_{dcn} = \frac{2\sqrt{2}}{\sqrt{3}} v_{n_{sac}}.$$

The application of this relation to the control system used in this work yields:

$$v_{dcn} = 677,69 \text{ V.}$$

The reference value of the v_{dc} verifies the following inequality.

$$v_{dc}^* < v_{dcn}.$$

In this work, the reference value of 600 V has been used.

Appendix 7: System nomenclature

| | |
|---------------------------|--|
| $\phi_r = \phi_{rd}$ | Rotor flux magnitude (Wb) |
| i_{sd}, i_{sq} | Stator currents components in in (d, q) coordinate frame (A) |
| v_{sd}, v_{sq} | Stator voltages in (d, q) coordinate frame (V) |
| n_p | Number of pole pairs |
| ω | Rotor electrical angular frequency (rad/s) |
| $\omega_m = \omega/n_p$ | Mechanical rotor speed (rad/s) |
| ω_s | Electrical angular frequency of the voltages and currents of stator windings (rad/s) |
| ω_r | Electrical angular frequency of the currents of rotor windings (rad/s) |
| θ_s | Stator electrical angular position (rad) |
| R_r, R_s | Rotor and stator resistances (Ω) |
| L_r, L_s | Rotor and stator inductances (H) |
| L_m | Mutual inductance (H) |
| R_L | Dump load resistance (Ω) |
| C | DC-link capacitor (F) |
| i_i | Current at the input of the inverter (A) |
| v_{dc} | DC-link voltage (V) |
| T_e | Electromagnetic torque (Nm) |
| $i_{s\alpha}, i_{s\beta}$ | Stator currents components in (α, β) coordinate frame (A) |
| $i_{r\alpha}, i_{r\beta}$ | Rotor currents components in (α, β) coordinate frame (A) |
| $v_{s\alpha}, v_{s\beta}$ | Stator voltages components in (α, β) coordinate frame (V) |
| S | Switching functions of PWM technique of Electronic Load Control (ELC) |
| S_a, S_b and S_c | Switching functions of PWM technique |

| | |
|------------------|--|
| S_d, S_q | Switching functions of PWM technique in (d, q) coordinate frame |
| ω_e | Pulsating frequency of the AC load (rad/s) |
| v_{id}, v_{iq} | Inverter output voltages components in (d, q) coordinate frame (V) |
| v_d, v_q | AC load voltages components in (d, q) coordinate frame (V) |
| i_{id}, i_{iq} | Inverter output currents components in (d, q) coordinate frame (A) |
| i_{Ld}, i_{Lq} | Load currents components in (d, q) coordinate frame (A) |
| R_f | LC-filter resistor in Inverter side (Ω) |
| L_f | LC-filter inductor in Inverter side (H) |
| C_f | LC-filter capacitor in Inverter side (F) |
| x^* | Reference signals for x . |

Appendix 8

(a, b, c) coordinate frame \rightarrow (α, β) coordinate frame equations [36].

$$\begin{bmatrix} x_\alpha \\ x_\beta \end{bmatrix} = \sqrt{\frac{2}{3}} \begin{bmatrix} 1 & -\frac{1}{2} & -\frac{1}{2} \\ 0 & \frac{\sqrt{3}}{2} & -\frac{\sqrt{3}}{2} \end{bmatrix} \begin{bmatrix} x_a \\ x_b \\ x_c \end{bmatrix}$$

(α, β) coordinate frame \rightarrow (d, q) coordinate frame equations.

$$\begin{bmatrix} x_d \\ x_q \end{bmatrix} = \begin{bmatrix} \cos \theta_s & \sin \theta_s \\ -\sin \theta_s & \cos \theta_s \end{bmatrix} \begin{bmatrix} x_\alpha \\ x_\beta \end{bmatrix}$$

(d, q) coordinate frame \rightarrow (α, β) coordinate frame equations.

$$\begin{bmatrix} x_\alpha \\ x_\beta \end{bmatrix} = \begin{bmatrix} \cos \theta_s & -\sin \theta_s \\ \sin \theta_s & \cos \theta_s \end{bmatrix} \begin{bmatrix} x_d \\ x_q \end{bmatrix}$$

(α, β) coordinate frame \rightarrow (a, b, c) coordinate frame equations.

$$\begin{bmatrix} x_a \\ x_b \\ x_c \end{bmatrix} = \sqrt{\frac{2}{3}} \begin{bmatrix} 1 & 0 \\ -\frac{1}{2} & \frac{\sqrt{3}}{2} \\ -\frac{1}{2} & -\frac{\sqrt{3}}{2} \end{bmatrix} \begin{bmatrix} x_\alpha \\ x_\beta \end{bmatrix}$$

Appendix 9

Design methodology for LC filter.

The transfer function of the second order low pass LC filter is

$$T(s) = \frac{1}{1 + R_f C_f s + L_f C_f s^2}.$$

The cut-off angular frequency of this filter is:

$$\omega_0 = \frac{1}{\sqrt{L_f C_f}}$$

The cut-off frequency is then equal to:

$$f_0 = \frac{1}{2\pi\sqrt{L_f C_f}}$$

The values of the LC filter can be chosen such that the central frequency of the first harmonic packet to be eliminated is equal to $5f_0$.

References

- Marino R, Peresada S, Tomei P (1995) Exponentially convergent rotor resistance estimation for induction motors. *IEEE Trans. Ind. Electron.* 42:508–515
- Ahmed-Ali T, Lamnabhi-Lagarrigue F, Ortega R (1999) A globally-stable adaptive indirect field-oriented controller for current-fed induction motors. *Int. J. Control* 72:996–1005
- Marino R, Peresada S, Tomei P (2000) On-line stator and rotor resistance estimation for induction motors. *IEEE Trans. Control Syst. Technol.* 8:570–579
- Akatsu K, Kawamura A (2000) On-line rotor resistance estimation using the transient state under the speed sensorless control of induction motor. *IEEE Trans. Power Electron.* 15:553–560
- Castaldi P, Geri W, Montanari M, Tilli A (2005) A new adaptive approach for on-line parameter and state estimation of induction motors. *Control Eng. Pract.* 13:81–94
- Marino R, Peresada S, Verrelli CM (2005) Adaptive control for speed-sensorless induction motors with uncertain load torque and rotor resistance. *Int. J. Adapt. Control Signal Process* 19:661–685
- Barut M, Bogosyan S, Gokasan M (2005) Speed sensorless direct torque control of induction motors with rotor resistance estimation. *Energy Convers Manag* 46:335–349
- Picardi C, Scibilia F (2006) Sliding-mode observer with resistances or speed adaptation for field-oriented induction motor drives. *IEEE Ind Electron IECON 2006*:1481–1486
- Koubaa Y (2006) Application of least-squares techniques for induction motor parameters estimation. *Math Comput Model Dyn Syst* 12:363–375
- Koubaa Y (2006) Asynchronous machine parameters estimation using recursive method. *Simul Model Pract Theory* 14:1010–1021
- Mezouar A, Fellah MK, Hadjeri S, Sahali Y (2006) Adaptive speed sensorless vector control of induction motor using singularly perturbed sliding mode observer. *IEEE Ind Electron IECON 2006*:932–939
- Castillo B, Gennaro SD, Loukianov A, Rivera J (2007) Robust nested sliding mode regulation with application to induction motors. In: *Proceedings of the 2007 American control conference*, New York City, USA, pp 5242–5247
- Roncero-Sánchez P, García-Cerraba A, Feliu-Batlle V (2007) Rotor resistance estimation for induction machines with indirect field-orientation. *Control Eng Pract* 15:1119–1133
- Wang K, Chiasson J, Bodson M, Tolbert LM (2007) An online rotor time constant estimator for the induction machine. *IEEE Trans Control Syst Technol* 15:339–348
- Mezouar A, Fellah MK, Hadjeri S (2008) Adaptive sliding-mode-observer for sensorless induction motor drive using two-time-scale approach. *Simul Model Pract Theory* 16:1323–1336
- Kenne G, Ahmed-Ali T, Lamnabhi-Lagarrigue F, Arzandé A (2008) Nonlinear systems time-varying parameter estimation: application to induction motors. *Electr Power Syst Res* 78:1881–1888
- Kenné G, Lamnabhi-Lagarrigue F (2012) Comparative study of two robust online rotor resistance estimators for induction machine adaptive control. In: *Proceedings of the IEEE international conference on industrial technology, special session paper*, Athens-Greece, 19–21 March, 2012, pp 437–442
- Louze L, Nemmour AL, Khezzer A, Hacil ME, Boucherma M (2009) Cascade sliding mode controller for self-excited induction generator. *Rev Energies Renouv* 12:617–626
- Seyoum D, Rahman MF, Grantham C (2003) Inverter supplied voltage control system for an isolated induction generator driven by a wind turbine. In: *38th IAS annual meeting conference record of the industry applications*, vol 1, pp 568–575
- Sivakami P, Karthigaivel R, Selvakumaran S (2013) Voltage control of variable speed induction generator using pwm converter. *Int J Eng Adv Technol* 2:2249–8958
- Benelghali S, Benbouzid ME Hachemi, Charpentier JF, Ahmed-Ali T, Munteanu I (2011) Experimental validation of a marine current turbine simulator: application to a permanent magnet synchronous generator-based system second-order sliding mode control. *IEEE Trans Ind Electron* 58:118–126
- Slootweg J, de Haan S, Polinder H, Kling W (2003) General model for representing variable speed wind turbines in power system dynamics simulations. *IEEE Trans Power Syst* 18:144–151
- Jaramillo-Lopez F, Kenne G, Lamnabhi-Lagarrigue F (2016) A novel online training neural network-based algorithm for wind speed estimation and adaptive control of pmsg wind turbine system for maximum power extraction. *Renew Energy* 86:38–48
- Mansour M, Nejib Mansouri M, Faouzi Mimouni M (2011) Comparative performance of fixed-speed and variable-speed wind turbine generator systems. *J Mech Eng Autom* 1:74–81
- Beltran B, Ahmed-Ali T, Benbouzid M (2009) High-order sliding mode control of variable speed wind turbines. *IEEE Trans Energy Convers* 56:3314–3321
- Slotine JJ, Li W (1991) *Applied nonlinear control*. Prentice Hall, New York
- Utkin VI (1992) *Sliding modes in optimization and control*. Springer, Berlin
- Leonhard W (1984) *Control of electric drives*. Springer, Berlin
- Levant A (1998) Robust exact differentiation via sliding mode technique. *Automatica* 34:379–384
- Kenne G, Ahmed-Ali T, Lamnabhi-Lagarrigue F, Arzandé A, Vanier JC (2011) An improved rotor resistance estimator for induction motors adaptive control. *Electr Power Syst Res* 81:930–941
- Haque M, Negnevitsky M, Muttaqi K (2008) A novel control strategy for a variable speed wind turbine with a permanent magnet synchronous generator. In: *2008 IEEE industry applications society annual meeting*, pp 1–8
- Liserre M, Blandjerg F, Hansen S (2005) Design and control of an LCL-filter-based three-phase active rectifier. *IEEE Trans Ind Appl* 41:1281–1291
- Beltran B, Ahmed-Ali T, Benbouzid M (2008) Sliding mode power control of variable speed wind energy conversion. *IEEE Trans Energy Convers* 23:551–558
- Bouafassa A, Rahmani L, Mekhilef S (2015) Design and real time implementation of single phase boost power factor correction converter. *ISA Trans* 55:267–274
- Shibashis B, van Zyl A, Spée R, Johan HRE (1997) Sensorless current control for active rectifiers. *IEEE Trans Ind Appl* 33:765–773
- Delaleau E, Louis JP, Ortega R (2001) Modeling and control of induction motors. *Int J Appl Math Comput Sci* 11:105–129